University of Ioannina

School of Sciences

Physics Department

Determination of mechanical quantities from the study of screw dislocations in Al, Cu (FCC) and W (BCC) from Molecular Dynamics Simulations

Master thesis

Author:

Kamila Savvidi

Supervisor:

Prof. Georgios Evangelakis

IOANNINA 2021

Acknowledgements

First of all, I would like to express my gratitude to my supervisor, Prof. George Evangelakis for the academic support and guidance, and, all the motivation he has given me during the last year. I am thankful to Prof. Vassilis Pontikis for the collaboration and valuable help in the present work. I thank also Prof. George Floudas for being in the examining jury. An the end, I thank Dr. Pablo Palomino for his help at the beginning of my thesis work.

Contents

Acknowledgements 1

1 Introduction **4**

2 Basic Elements on the Theory of Elasticity **6**

2.1 Strain tensor 6

2.2 Stress tensor 7

2.3 Elastic energy 9

2.4 Elastic constants 10

2.5 Elasticity theory of isotropic solids 11

3 Introduction to dislocation theory **13**

3.1 Geometry of dislocations 13

3.2 Burgers vector and Burgers circuit of a dislocation 14

3.3 Glide 15

3.4 Screw dislocation 16

3.5 Strain energy of a dislocation 17

3.6 Forces on dislocations 18

3.7 Dislocations in FCC metals & Stacking fault 18

3.8 Dislocations in BCC metals 20

3.8.1 Stacking sequence on {110} planes 21

3.8.2 Stacking sequence on {112} planes 21

4 Molecular dynamics **23**

4.1 Why simulations 23

4.2 Molecular Dynamics 24

4.3 Verlet algorithm 26

4.4 Interatomic potential - TBSMA 26

4.5 Boundary conditions . . . 28
4.6 Statistical ensembles. Thermostat and Barostat . . . 29

5 Method-Computational details **31**
5.1 Computational details . . . 31
5.2 Results . . . 32
5.2.1 Aluminium (fcc) . . . 32
5.2.2 Copper (fcc) . . . 39
5.2.3 Tungsten (bcc) . . . 45
5.3 Discussion . . . 50

6 Concluding remarks **53**

A General case **54**

A Tungsten Potential **55**

Bibliography **56**

List of Figures **60**

List of Tables **63**

Chapter 1

Introduction

The elastic constants are an important property of the material. They determine the behavior of materials under arbitrary, fairly small deformations. Over the last decades several simulation methods have be been developed based on an atomistic arrangement and a given interatomic interaction. There are several approaches to calculate the elastic constants of a material, using strain fluctuation methodology, from the strain-stress curve under applied stress or from the central difference of elastic energy. In the first, displacement and, therefore, strain is calculated in comparison to a reference state and then elastic stiffness constants are obtained through a transformation of the elastic compliance constants. The method of using strain fluctuations has evolved and yields the elastic constants run in different thermodynamic ensembles. The withdraw is the time-consuming convergence and the accuracy that is limited mainly at low temperatures. Also under certain temperature and pressure conditions, strain fluctuations can be enhanced if Born stability criteria are not satisfied. [1, 2, 3, 4] In the strain-stress curve method, for every elastic constant an appropriate strain (or stress) have to applied. Also, this method can be problematic because of the possibility of setting up a plastic flow in the system. [5]. Additionally, elastic constants can be obtained by applying strain and calculating the elastic constants with respect to the second derivative of elastic energy but this method is limited only at the temperature of 0K.

All real crystals contain imperfections which may be point, line, surface or volume defects and which disturb the perfect arrangement of atoms. In this work, line defects, the so-called *dislocations* are considered. Their modern study began independently in 1934 by Orowan, Polanyi and Taylor [6, 7, 8] in an attempt to reconcile the theoretical and experimental values of the applied shear stress required to plastically deform a single crystal. Plastic deformation occurs by the glide of dislocations and hence the critical shear stress for the onset of plastic deformation is the stress required to move dislocations. Thus, a study of dislocations and their associate quantities are of great interest.

The atomistic simulations of individual dislocations require special treatment due to the long-ranged field associated with them. Fixed Boundary Conditions (FBC) have been used in dislocation simulations, where the exterior atoms of the simulation cell are frozen to their lattice positions. This requires very large simulation cells and, therefore, computational memory requirements and time. Also, this method is problematic because of the force built-up between fixed and relaxed atomic regions. To get rid of the external boundary in all three directions, one can use Periodic Boundary Conditions (PBC) but the dislocation should be introduced in the simulation cell as dislocation dipole, i.e. two dislocations with opposite Burgers vectors. This way, the stress of these two dislocations will cancel at long distances as well as the elastic interaction with image dislocations that appear because of the PBC. [9] Also, dislocation loss is also a possible impementation due to the fact that dislocations glide at finite temperature and can be absorbed by the boundary. In this work, Helicoidal Boundary Conditions (HBC) are originally applied in dislocation simulation that overcome the aforementioned implementations.

The presence of dislocations create an elastic field around the dislocation that is declining inversely proportional to the distance ($\sim 1/r$). The atoms near the core of the dislocation, i.e. the region in the immediate vicinity of the line defect, are extremely distorted relatively to their normal lattice position, and the result is the accumulation of elastic energy in the body. The excess of elastic strain energy has logarithmic dependence on the distance from the dislocation core. In the present thesis, we introduced perfect screw dislocations in aluminum (Al), copper (Cu) and tungsten (W) to calculate the shear modulus. Additionally, the elastic constants C_{44} either for the isotropic case of Al and W or anisotropic case of Cu were obtained. In the case of fcc metals, where the screw dislocation dissociates into co-planar partial screw dislocation, the intristic stacking fault energy γ was calculated. In addition, we use a new potential interatomic potential for W that is proved to be a very realistic approach for, otherwise, very difficult to describe semi-empirically.

Chapter 2

Basic Elements on the Theory of Elasticity

Solid bodies are said to be *strained* when the relative positions of points in the medium are altered . The change in the position of the material points, when accompanied by a change in the distance between them, is called *deformation*. When a body is deformed forces arise, called *internal stresses*, that tend to return the body to equilibrum. Stress is linearly related to strain for small destortions via *elastic stiffness constants*. Solids possessing symmetry, i.e. cubic symmetry, can have reduced number of elastic constants. For isotropic solids the number of elastic constants is further reduced to only two elastic constants.

2.1 Strain tensor

The position of any point in the solid is defined by its radius vector r (with components x_i) in a coordinate system embedded in the body. The deformation of a body is described with the strain tensor in the following way. Let a certain point have a radius vector r before deformation, and after the deformation have a different value r' with components x'_i. [10] [11] The *displacement vector* is defined

$$u_i = x'_i - x_i \tag{2.1}$$

Let us consider two points close together. If the radius vector joining them before the deformation is dx_i, then the radius vector joining them in the deformed body would be $dx'_i = dx_i + du_i$. The distance between the two points is $dl^2 = dx_i^2$ and $dl'^2 = dx'^2_i = (dx_i + du_i)^2$ respectively, where the summation over i is

implied. Substituing $du_i = (\partial u_i/\partial x_k)dx_k$, we can write

$$dl'^2 = dl^2 + 2\frac{\partial u_i}{\partial x_k}dx_i dx_k + \frac{\partial u_i}{\partial x_k}\frac{\partial u_i}{\partial x_l}dx_k dx_l \tag{2.2}$$

The summation is taken over both suffixes i and k in the second term, thus we can write $\partial u_k/\partial x_i dx_i dx_k$ instead. In the third term, we interchange the suffixes i and l. Then dl^2 takes the final form

$$dl'^2 = dl^2 + 2\epsilon_{ik}dx_i dx_k$$

where the tensor is defined as

$$\epsilon_{ik} = \frac{1}{2}(\frac{\partial u_i}{\partial x_k} + \frac{\partial u_k}{\partial x_i} + \frac{\partial u_l}{\partial u_i}\frac{\partial u_l}{\partial u_k}) \tag{2.3}$$

The tensor ϵ_{ik} is called the *strain tensor*. By definition it is a symmetrical tensor, therefore it can be diagonalised at any given point by choosing co-ordinate axes so that only the diagonal components $\epsilon_{11}, \epsilon_{22}, \epsilon_{33}$ are non-zero. Each of these strains is a simple extension (or compression) in the corresponding direction.
In practice for almost all cases, the strains are small. This means that the relative extensions are very small compared with unity. Thus for small deformations, the third term will be neglected as being of second-order. This procedure results in linear theory of elasticity, which is a good approximation for small displacements.

In general, the strain tensor is given

$$\epsilon_{ik} = \frac{1}{2}(\frac{\partial u_i}{\partial x_k} + \frac{\partial u_k}{\partial x_i}) \tag{2.4}$$

For the off-diagonal components, $i \neq j$, that is, for *shear strains* Eq.(2.4) gives only half the shear strain, as usually defined in engineering,

$$\gamma_{ij} = 2\epsilon_{ij}, i \neq j$$

As showm in Figure 2.1, shear strain $\gamma_{ij} = \phi_1 + \phi_2$ can be interprented as the angle of shear.

2.2 Stress tensor

When a body is not deformed, all parts of the body are in mechanical equilibrium. When deformation occurs, the arrangement of the atoms is changed, and the body ceases to be in its initial state of equlibrium. Forces therefore arise which tend to return the body to equilibrium. The internal *forces per area*, due to molecular

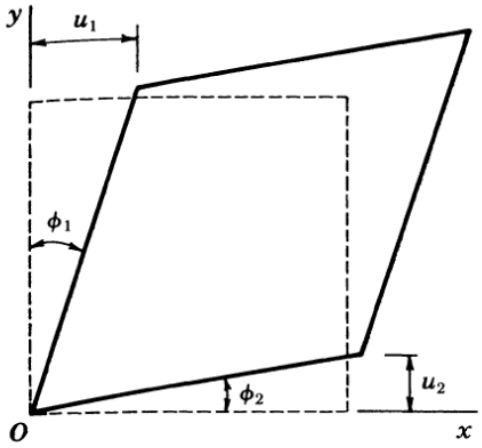

Figure 2.1: Shear displacements u_1 and u_2 and angles of shear ϕ_1 and ϕ_2 [9]

forces (i.e. interatomic forces) which occur when a body is deformed are called *internal stresses*.

Molecular forces are short range, their effect extends to a distance as betweeen atoms. In the theory of elasticity, the distances considered are much greater compared to distances between atoms, therefore the forces exerted on any part of the body by surrounding parts act only of the surface of that part.

Let us consider the total force on some portion of a body. It is the sum of all the forces on all volume elements in that portion of the body, $\int \mathbf{F}\ dV$, where $\vec{F}$ is the force per unit volume and $\mathbf{F}dV$ the force on the volume element dV. With the above discussion, however, all these forces act on the surface of that portion, and so the resultant force can be represented as the sum of forces acting on all the surfaces elements, i.e. as an intergral over the surface.

$$\int \mathbf{F}dV = \int \frac{\partial \sigma_{ik}}{\partial x_k} dV = \oint \sigma_{ik} df_k$$

The tensor σ_{ik} is called the *stress tensor*. The $\sigma_{ik}df_k$ is the i-th component of the force on the surface element perpendicular to the x_k-axis.

Stress tensor is also symmetrical $\sigma_{ij} = \sigma_{ji}$. At rest, each volument element of the solid must be in mechanical equilbrium. There are no torque on the element as a consequence of the symmetry of stress tensor. Also, no net force can act on the element, so that

$$\frac{\partial \sigma_{ij}}{\partial x_j} + f_i = 0 \tag{2.5}$$

where f_i is the ith component of the body force per unit volume.

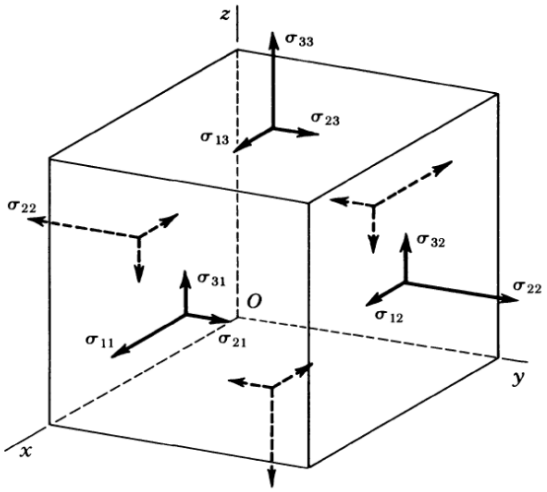

Figure 2.2: Stress distribution on a infitensimal volume element [9]

2.3 Elastic energy

For small distortions stresses depend linearly on deformation

$$\sigma_{ij} = C_{ijkl}\epsilon_{kl} \tag{2.6}$$

The coefficients C_{ijkl} are called the elastic constants. By virtue of both strain and stress tensor, it follows that

$$C_{ijkl} = C_{jikl} = C_{ijlk} = C_{jilk} \tag{2.7}$$

Substituting Eq.(2.4) and Eq. (2.6) into Eq. (2.5) yields the expression

$$\sigma_{ij} = C_{ijkl}\frac{\partial u_l}{\partial u_k} \tag{2.8}$$

The further substitution of Eq.(2.8) into (2.5) gives

$$C_{ijkl}\frac{\partial^2 u_k}{\partial x_j \partial x_l} + f_i = 0 \tag{2.9}$$

We suppose that the deformation process occurs so slowly that is thermodynamically reversible. Then the elastic strain energy is given by the work done on that element by the stresses acting

$$dW = \sigma_{ij}d\epsilon_{ij} = C_{ijkl}\epsilon_{kl}d\epsilon_{ij}$$

The Helmholtz free energy for a reversible and isothermal change is

$$dF = -SdT + dW$$

If the deformation is reversible and isothermal, and if the work done is, in general, restricted to that of elastic deformation, the differential work is equal to the differential change in Helmholtz free energy

$$dF = dW = C_{ijkl}\epsilon_{kl}d\epsilon_{ij} \tag{2.10}$$

Thus,

$$\frac{\partial^2 F}{\partial\epsilon_{ij}\partial\epsilon_{kl}} = C_{ijkl} \tag{2.11}$$

The free energy is a function of state and dF is a exact differential, so that the order of differentation in Eq. (2.11) is immaterial. Hence, Eq.(2.11) indicates that

$$C_{ijkl} = C_{klij} \tag{2.12}$$

The strain energy-density is determined from Eq. (2.10) to be

$$w = \frac{1}{2}C_{ijkl}\epsilon_{ij}\epsilon_{kl} \tag{2.13}$$

2.4 Elastic constants

The C_{ijkl} is a 9x9 matrix. Direct consequence of the symmetry in strain and stress tensor is that only 36 out of 81 components of the *elastic stiffness tensor* are independent and distinct terms. Additional simplification of the stress-strain relationship can be realized through simplification of the matrix notation. It is common for elastic constants to be written in a contracted form as C_{mn}, where m and n are each indices corresponding to a pair of indices ij and kl, as followed :

ij	or	kl	11	22	33	23	31	12	32	13	21
m	or	n	1	2	3	4	5	6	7	8	9

Of the 36 elastic constants, there are six constants where $m = n$, leaving 30 constants where $m \neq n$. Only one-half of these are independent due to symmetry $C_{mn} = C_{nm}$ (Eq. (2.12)), thus for the general anisotropic linear elastic solid there 21 independent elastic constants. It is usually written in the following 6x6 representation where γ_{ij} are used for shear strains instead of ϵ_{ij} :

$$\begin{bmatrix} \sigma_{11} \\ \sigma_{22} \\ \sigma_{33} \\ \sigma_{23} \\ \sigma_{31} \\ \sigma_{12} \end{bmatrix} = \begin{bmatrix} C_{11} & C_{12} & C_{13} & C_{14} & C_{15} & C_{16} \\ C_{12} & C_{22} & C_{23} & C_{24} & C_{25} & C_{26} \\ C_{13} & C_{23} & C_{33} & C_{34} & C_{35} & C_{36} \\ C_{14} & C_{24} & C_{34} & C_{44} & C_{45} & C_{46} \\ C_{15} & C_{25} & C_{35} & C_{45} & C_{55} & C_{56} \\ C_{16} & C_{26} & C_{36} & C_{46} & C_{56} & C_{66} \end{bmatrix} \begin{bmatrix} \epsilon_{11} \\ \epsilon_{22} \\ \epsilon_{33} \\ \gamma_{23} \\ \gamma_{31} \\ \gamma_{12} \end{bmatrix} \tag{2.14}$$

Cubic crsytals

The number of independent elastic stiffness constants are further reduced because of crystal symmetry. In the case of cubic crystal there are only three independent elastic stiffness constants. Let the coordinate axes be parallel to the cube edges. In Eq. (2.14) we must have: $C_{11} = C_{22} = C_{33}, C_{12} = C_{23} = C_{13}, C_{44} = C_{55} = C_{66}$ due the fact that x,y and z axes are identical by 90° rotations. Also the off-diagonal shear components are zero, ie. $C_{45} = C_{56} = C_{46}$, and mixed compression/shear does occur, i.e. $C_{14} = C_{24} = ... = 0$. Therefore, the cubic elasticity matrix is

$$C_{mn} = \begin{bmatrix} C_{11} & C_{12} & C_{12} & 0 & 0 & 0 \\ C_{12} & C_{11} & C_{12} & 0 & 0 & 0 \\ C_{12} & C_{12} & C_{11} & 0 & 0 & 0 \\ 0 & 0 & 0 & C_{44} & 0 & 0 \\ 0 & 0 & 0 & 0 & C_{44} & 0 \\ 0 & 0 & 0 & 0 & 0 & C_{44} \end{bmatrix} \tag{2.15}$$

and the relation between σ and ϵ from Eq (2.14) and Eq.(2.15) are:

$$\begin{aligned} \sigma_{11} &= C_{11}\epsilon_{11} + C_{12}\epsilon_{22} + C_{12}\epsilon_{33} \qquad & \sigma_{23} &= 2C_{44}\epsilon_{23} \\ \sigma_{22} &= C_{12}\epsilon_{11} + C_{22}\epsilon_{22} + C_{12}\epsilon_{33} \qquad & \sigma_{31} &= 2C_{44}\epsilon_{31} \\ \sigma_{33} &= C_{12}\epsilon_{11} + C_{12}\epsilon_{22} + C_{11}\epsilon_{33} \qquad & \sigma_{12} &= 2C_{44}\epsilon_{12} \end{aligned} \tag{2.16}$$

2.5 Elasticity theory of isotropic solids

If the medium is elastically isotropic, i.e. the elastic properties are independent of the directions, only two independent constants are required. Let only $\epsilon_{11} \neq 0$, so that Eq. (2.16) gives

$$\sigma_{11} = C_{11}\epsilon_{11}$$
$$\sigma_{22} = \sigma_{33} = C_{12}\epsilon_{11} = \frac{C_{12}}{C_{11}}\epsilon_{11}$$

The transformation matrix to rotate the cooordinate system 45° about z axis is:

$$T_{ij} = \begin{bmatrix} \frac{\sqrt{2}}{2} & \frac{\sqrt{2}}{2} & 0 \\ -\frac{\sqrt{2}}{2} & \frac{\sqrt{2}}{2} & 0 \\ 0 & 0 & 1 \end{bmatrix}$$

Strain and stress transforms the following way

$$\epsilon'_{12} = T_{11}T_{12}\epsilon_{11}$$

$$\sigma'_{12} = -\frac{1}{2}\sigma_{11} + \frac{1}{2}\sigma_{22} = -\frac{1}{2}C_{11}\epsilon_{11} + \frac{1}{2}C_{12}\epsilon_{11} = (C_{11} - C_{12})\epsilon'_{12}$$

But from Eq. (2.16), $\sigma'_{12} = 2C_{44}\epsilon'_{12}$, so that

$$(C_{11} - C_{12}) = 2C_{44}$$

and only two of three elastic constants are independent. For anisotropic cubic crystals, the *anisotropy ratio* is defined

$$A = \frac{2C_{44}}{C_{11} - C_{12}}$$

For isotropic materials $A = 1$ and for anisotropic materials the degree of anisotropy is measured by the deviation of A from unity. When this condition is satisfied, it is usual to express Eq. (2.16) in terms of the two elastic constants λ (the Lame constant) and G (the shear modulus)

$$\begin{aligned} \sigma_{11} &= 2G\epsilon_{11} + \lambda(\epsilon_{11} + \epsilon_{22} + \epsilon_{33}) \quad \sigma_{12} = 2G\epsilon_{12} \\ \sigma_{22} &= 2G\epsilon_{22} + \lambda(\epsilon_{11} + \epsilon_{22} + \epsilon_{33}) \quad \sigma_{23} = 2G\epsilon_{23} \\ \sigma_{33} &= 2G\epsilon_{33} + \lambda(\epsilon_{11} + \epsilon_{22} + \epsilon_{33}) \quad \sigma_{13} = 2G\epsilon_{13} \end{aligned} \tag{2.17}$$

Chapter 3

Introduction to dislocation theory

Metals and many important non-metallic classes of solids are crystalline, i.e. the constituent atoms are arranged in a regular sequence that repeats itself periodically in three dimensions. The actual arrangement of the atoms is described by the crystal structure. The crystal strucures of most pure metals are relatively simple. The most common are the body-centered cubic, face-centered cubic and close-packed hexagonal.
Real crystals contain imperfections; dislocations are linear defects, around which atoms of the crystal lattice are misaligned. There are two basic types of dislocations, the edge dislocation and the screw dislocation. In this chapter basic concepts of dislocations are introduced. The strain and stress of a scew dislocation is derived, as well as the strain energy. Furthermore, slip and dissociation of dislocations are presented for fcc and bcc metals.

3.1 Geometry of dislocations

Figure 3.1 depicts a simplified descriptive model of the atomic arrangement and bonding in a simple cubic structure. For convenience it is assumed that the bonds can be represented by flexible springs between adjacent atoms. Neverthelesss, bonding in real solids is complex and the nature of bonds can determine the equilibrium positions of atoms. Edge dislocation can be represented in the following way: all the bonds across the surface ABCD are broken and the faces of the crystal are separated so that an extra half-plane of atoms can be inserted in between. The only large distortion of the atoms from their normal positions relative to their neighbors is close to the line DC. The region of irregularity extends few lattice periods and decrease with increasing distance from the line. The line DC is an edge dislocation.
A screw dislocation can be obtained by displacing the crystal on one side of ABCD relative to the other side in the direction AB as in Figure 3.2. The presence of a straight screw dislocation transforms the crystal

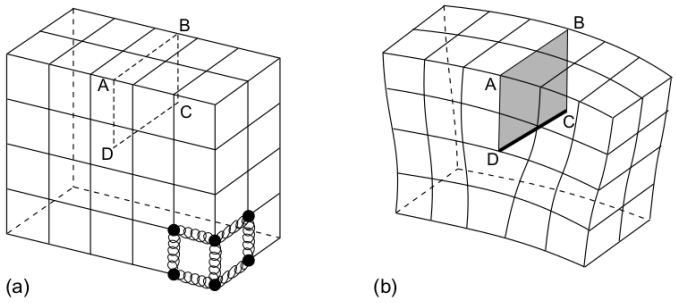

Figure 3.1: (a) Model of simple cubic lattice (b) Edge dislocation DC formed by inserting an extra half-plane of atoms in ABCD [12]

planes into a helicoidal surface. The line DC is a screw dislocation. Looking down the dislocation line, if the helix advances one plane when a clockwise circuit is made round, it is referred to as right-handed screw dislocation, and if the reverse is true it is a left-handed.

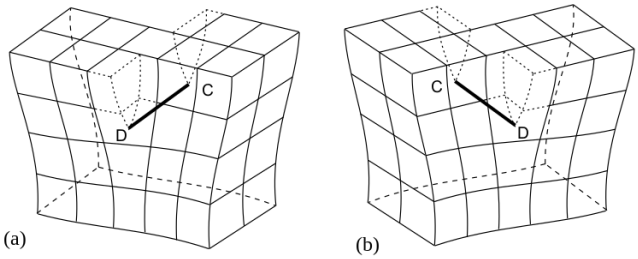

Figure 3.2: (a) A left-hand screw dislocation (b) A right-hand screw dislocation [12]

3.2 Burgers vector and Burgers circuit of a dislocation

We consider a dislocation in a simple cubic lattice as in Figure 3.1. Figure 3.3 shows a section normal to a cube plane intersected by an edge dislocation and a perfect reference lattice, where the translation vector $mt_1 + nt_2$, with $m = 1, 2, 3,\ n = 1, 2, 3$. After passage around any closed atom-to-atom loop that encircles the dislocation line the displacement vector to enclose the loop in the perfect reference lattice receives a certain increment b, called the *Burgers vector*, which is equal to one of the lattice vectors in magnitude and direction. We define the sense of the dislocation line by assigning a unit vector $\vec{\xi}$ parallel to the dislocation line and taking the positive sense in the direction of $\vec{\xi}$. Burgers vector now can be defined by the procedure illustrated in Figure 3.3, where the positive sense of $\vec{\xi}$ is taken to be into the paper.

For a Burgers circuit enclosing a screw dislocation the Burgers vector is parallel to the dislocation line sense. Thus:

a) The Burgers vector of an edge dislocation is normal to the line of the dislocation.

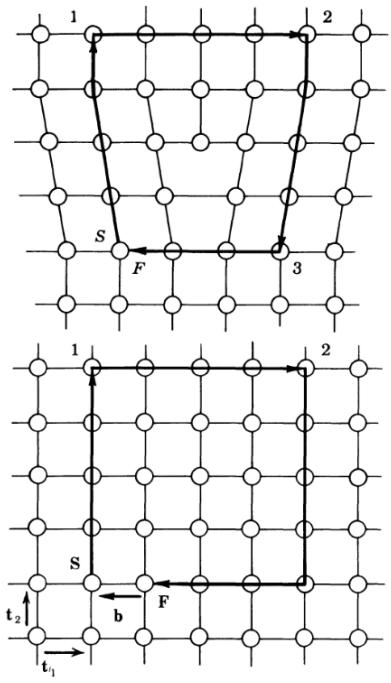

Figure 3.3: Burgers circuit about an edge dislocation [9]

b) The Burgers vector of a screw dislocation is parallel to the line of the dislocation.

In general the dislocation line lies in an arbitrary angle to its Burgers vector and the dislocation has a mixed edge and screw character.

3.3 Glide

Dislocations move under internal or applied stress. *Glide* occurs when the dislocation moves in the surface that contains both its line and Burgers vector. Glide of many dislocations results in *slip*, which is one of the main mechanisms of plastic deformation in crystalline solids. It can be envisaged as sliding of one plane of atoms over another.

The slip planes are normally the planes with the highest density of atoms and the direction of slip is the direction in the slip plane corresponding to one of the shortest lattice translation vectors.

The glide plane of an edge dislocation is normal to plane defined by the dislocation line and the Burgers vector $\vec{b} \times \vec{\xi}$.For a screw dislocation, however, where $\vec{b}$ is parallel to $\vec{\xi}$, $(\vec{b} \times \vec{\xi} = 0)$, any plane for which $\vec{b}$ is a zone axis is a possible glide plane.

3.4 Screw dislocation

The elastic distortion of an infinitely-long straight dislocation can be represented in terms of a cylinder of material. In Figure 3.4 (a) there is a screw dislocation AB; the cylinder in Figure 3.4 (b) has been deformed to produce a similar distortion.

The elastic field in the dislocated cylinder can be found directly. There are no displacements in the x and y directions $u_x = u_y = 0$. The displacement in the z-direction increases from zero to b as θ increases from 0 to 2π :

$$u_z = \frac{b\theta}{2\pi} = \frac{b}{2\pi}\arctan(y/x)$$

It is found from Eq. (1.4) that

$$\begin{aligned} \epsilon_{xx} = \epsilon_{yy} = \epsilon_{zz} = \epsilon_{xy} = \epsilon_{yx} = 0 \\ \epsilon_{xz} = \epsilon_{zx} = -\frac{b}{4\pi}\frac{y}{x^2+y^2} = -\frac{b}{4\pi}\frac{sin\theta}{r} \\ \epsilon_{yz} = \epsilon_{zy} = \frac{b}{4\pi}\frac{x}{x^2+y^2} = \frac{b}{4\pi}\frac{cos\theta}{r} \end{aligned} \tag{3.1}$$

From Eq (1.16) and Eq. (1.17), the components of stress are

$$\begin{aligned} \sigma_{xx} = \sigma_{yy} = \sigma_{zz} = \sigma_{xy} = \sigma_{yx} = 0 \\ \sigma_{xz} = \sigma_{zx} = -\frac{Gb}{2\pi}\frac{y}{x^2+y^2} = -\frac{Gb}{2\pi}\frac{sin\theta}{r} \\ \sigma_{yz} = \sigma_{zy} = \frac{Gb}{2\pi}\frac{x}{x^2+y^2} = \frac{Gb}{2\pi}\frac{cos\theta}{r} \end{aligned} \tag{3.2}$$

It is practical to write the stress components in cylindrical polar coordinates using the relations

$$\begin{aligned} \sigma_{rz} = \sigma_{xz}\cos\theta + \sigma_{yz}\sin\theta \\ \sigma_{\theta z} = -\sigma_{xz}\sin\theta + \sigma_{yz}\cos\theta \end{aligned} \tag{3.3}$$

and similarly for the shear strains, the only non-zero components are found to be

$$\begin{aligned} \epsilon_{\theta z} = \epsilon_{z\theta} = \frac{b}{4\pi r} \\ \sigma_{\theta z} = \sigma_{z\theta} = \frac{Gb}{2\pi r} \end{aligned} \tag{3.4}$$

K

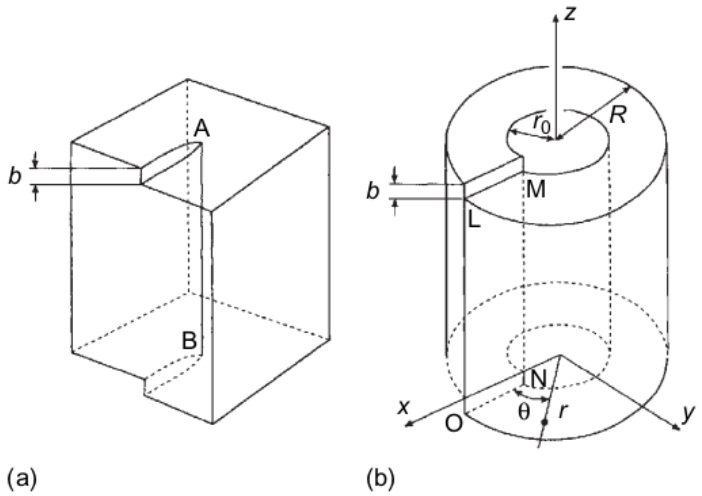

Figure 3.4: (a) Screw dislocation AB formed in a crystal (b) Elastic distortion of a cylindrical tube simulating the distortion produced by the screw dislocation [12]

3.5 Strain energy of a dislocation

The existence of distortion around a dislocation implies that a crystal is not its lowest energy state. The total strain energy is divided into two parts

$$E_{total} = E_{core} + E_{elasticstrain} \tag{3.5}$$

The elastic part, stored outside the core, may be determined by intergration of Eq. (1.13) for each small element of volume that for a screw dislocation is cylidrical shell of radius r and thickerss dr. The elastic strain energy stored in this volume *per length of dislocation* is

$$dE_{el}(screw) = \frac{1}{2} 2\pi r dr(\sigma_{\theta z}\epsilon_{\theta z} + \sigma_{z\theta}\epsilon_{z\theta}) = 4\pi r dr G\epsilon_{\theta z}^2 \tag{3.6}$$

Thus, by replacing the strain of screw dislocation in the above equation, the total elastic energy stored in the cylinder (Figure 3.4) per unit length of dislocation is

$$E_{el}(screw) = \frac{Gb^2}{4\pi}\int_{r_0}^{R}\frac{dr}{r} = \frac{Gb^2}{4\pi}\ln(\frac{R}{r_0}) \tag{3.7}$$

where R is the outer radius and r_0 is the core radius. The energy $E_{el(screw)}/L$ diverges as $R \to \infty$ or as $r_0 \to 0$. The divergence with R shows one cannot ascribe a definite characteristic energy to the dislocation; the energy depends on the size of the crystal. The divergence with r_0 arises becauses linear elasticity theory ceases to be valid due the extreme lattice distortion near the core of the dislocation. Therefore the intergral is taken from r_0 to the outer radius. A reasonable value for *dislocation core radius* lies in the range b to $4b$.

The elastic strain energy of an edge dislocation are

$$E_{el}(edge) = \frac{Gb^2}{4\pi(1-\nu)} \ln(\frac{R}{r_0}) \tag{3.8}$$

The elastic strain energy of a mixed dislocation can be written as the superposition of the screw and edge counterparts. The energy per unit length is relatively insensitive to the type of the dislocation and the values of R and r_0 because of the logarithmic dependence, thus, all equations can be approximately written

$$E_{el} = \alpha G b^2 \tag{3.9}$$

where $\alpha \approx 0.5 - 1.0$. This leads to Frank's rule; that two dislocations react and combine if it is energetically favorable. If $(b_1^2 + b_2^2 > b_3^2)$ then the reaction is favorable. If $(b_1^2 + b_2^2 < b_3^2)$ the reaction is unfavorable and the dislocation with Burgers vector dissociates into partial dislocations.

3.6 Forces on dislocations

Forces on dislocations are virtual. Applied stress does work on a crystal when a dislocation moves; the dislocation responds to the stress as it experiences a force equal to the work done divided by the distance it moves. The force between two dislocations is determined from the work done of introducing a dislocation in a crystal against the stresses of another dislocation present. [13] [peach and]
The force $\vec{F}$ acting on a dislocation of length L can be obtained from relation

$$\vec{F} = (\vec{b} \cdot \bar{\bar{\sigma}}) \times \vec{L} \tag{3.10}$$

3.7 Dislocations in FCC metals & Stacking fault

The geometry of a close packed plane of hard spheres such as the (111) plane in an fcc crystal is shown in Figure 3.5. We can distinguish two kinds of hollows in such a plane; we call them arbitrarily B and C. The next layer in a closed packed stacking will now fill either all the B hollows or all the C hollows. Two hollows of the same nature are separated by the vector of the type $\frac{1}{2}[110]$. If such two layers are to glide one with respect to the next one, perfect register is achieved after glide over a vector of the type $\frac{1}{2}[110]$ (Amelinckx citation).
According to dislocation theory this glide motion is performed by the movement of a dislocation with Burgers vector $\vec{b_1} = \frac{1}{2}[110]$. It is energetically more favorable to perform this motion in two steps: the first step leading to an intermediate position, whereby the atom occupies the wrong type of hollow, the second step brings the layer in the right type of hollows.(Heiderich, Schockley) In this way atoms from B site instead

of moving over the top of A atoms (vector $\vec{b_1}$) will move first to the nearby C site along the 'valley' between the two A atoms (vector $\vec{b_2}$) the then to the new B site via a second 'valley' (vector $\vec{b_3}$).

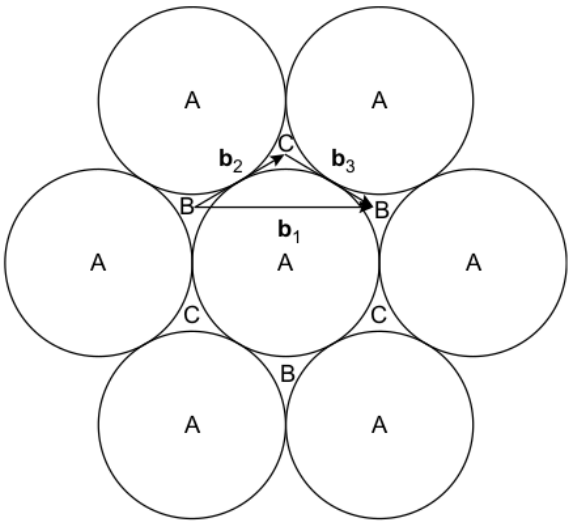

Figure 3.5: Slip of {111} planes in face-centeed cubic metals [12]

Thus the perfect dislocation splits into two *partial dislocations*. Partials dislocations of the type $\frac{1}{2} < 112 >$ which are glissile in the {111} planes are called *Schockley partials*.

The region between the two partial dislocations is faulted, since the top layer occupies the wrong family of hollows. The region in the faulted region between the two partials then becomes

$$...ABCA\mathbf{BCBC}ABA...$$

it contains a triplet in the hexagonal arrangement $..BCBC..$. The dislocations with Burgers vector $\vec{b_2} = \frac{1}{2}[2\bar{1}\bar{1}]$ and $\vec{b_3} = \frac{1}{2}[11\bar{2}]$ are called partial since they are not lattice vectors.

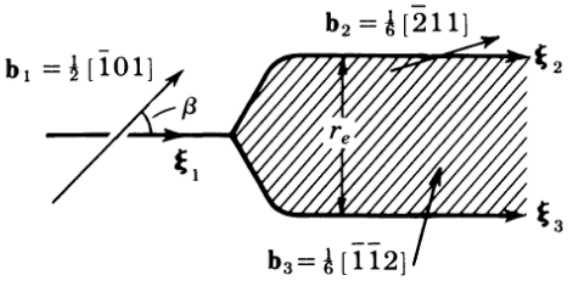

Figure 3.6: Dissociation of a perfect dislocation into Shockley partials [9]

Frank's rule shows that the reaction is energetically favorable, for from $\vec{b_1}^2 = a^2/2$ which is greater than $\vec{b_2}^2 + \vec{b_3}^2 = a^2/3$. The two partial dislocations with Burgers vector $\vec{b_2}$ and $\vec{b_3}$ repel each other. In contrast, if the partials move apart from each other, they increase the surface of the stacking fault and increase the stacking fault energy, which amounts to $E = \gamma r$ per unit length of dislocation are separated by r. The restoring force $-\partial E/\partial r = -\gamma$ is attractive.

Equilibrating this repulsive force with the attractive stacking fault leads to stable equilibrium distance between partials

$$r_e = \frac{Gb_1^2}{8\pi\gamma}\frac{2-\nu}{1-\nu}(1 - \frac{2\nu cos2\beta}{2-\nu}) \tag{3.11}$$

As shown in Figure 3.6 the angle β is between perfect screw dislocation and its line sense, ν is Poisson's ratio and b_1 the Burgers vector of the perfect screw dislocation.

3.8 Dislocations in BCC metals

The dislocation geometry in the body-centered cubic crystals differs from that in the face-centered cubic crystals. The dislocation core structure in BCC metals are not dictated by geometry alone, but are influenced also by the potential.

The shortest lattice vectors in BCC metals are of the $\frac{\alpha}{2}[111]$ type, and slip is indeed observed to occur in the [111] direction. There have been also observed dislocations of the [100] type, but those are thought to be products of reactions between $\frac{1}{2}[111]$ dislocations. The most widely spaced atomic planes in bcc metals are the {110} planes. It has been generally observed that slip occurs most actively in {110} planes. [14] However, slip on {112} and even {123} planes has been also observed at higher temperatures, as {112} planes have the second largest spacing and {123} planes rank the third among the planes that contain the [111] direction.

Screw dislocations in bcc metals do not dissociate into a plane, as in fcc metals, because there are no stable stacking faults in bcc metals. Various variants of screw dislocation splitting were considered. [15] Eventually, with the help of computer simulations, a three-way dissociation into three equivalent {110} planes emerged. Vitek et al. [16] and Duesbery et al. [17],[18] have shown that such a dissociation can occur even when no plane of the zone contain a stable stacking fault. Therefore, the term "dissociation" implies that the perfect screw dislocation somehow splits into several partial dislocations.

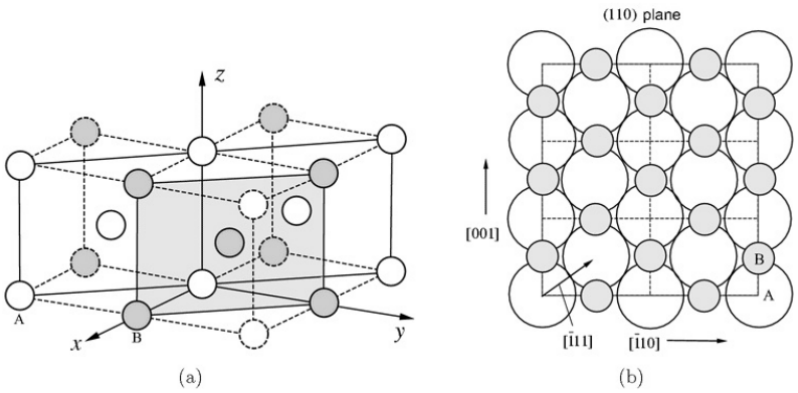

Figure 3.7: Stacking of BCC structure (a) Three-dimensional view (b) Plan view [19]

3.8.1 Stacking sequence on {110} planes

In Figure 3.7 (a) we see three adjacent unit cells of the bcc crystal structure. The atoms on each (110) plane form a centered-rectangle lattice. The atomic layer, labelel as A, passing through the origin is shown as white spheres with solid borders and the next atomic layer, labeled as layer B, in the [110] direction is shown as gray spheres with solid borders. The entire bcc crsytal structure can be considered as (110) atomic layers stacked on top of each other in the sequence ABAB... . The Figure 3.7 (b) showsthe bcc crystal structure viewed in the [110] direction. Layer B is displaced from layer A in out-of-plane direction by $\alpha/sqrt2$, where α is the lattice constant.

3.8.2 Stacking sequence on {112} planes

Figure 3.8 shows a set of $(1\bar{1}2)$ atomic planes in a bcc crystal. There are six types of $(1\bar{1}2)$ layers,stacked ontop of each oher in a periodic pattern of ABCDEFABCDEF... . Figure 3.9 a has the same viewing direction as that used in Figure 3.7 b. White atoms are in the plane of the paper, and the coordinates of the gray atoms have an out-of-plane component of $\frac{\alpha}{2}$. The dashed lines represent the $(1\bar{1}2)$ of Figure 3.8 and the horizontal axis is along the $[\bar{1}11$ direction.

Suppose that layer B (together with all layers above it) slips relative to layer A by $\frac{\alpha}{6}[\bar{1}11]$, then it becomes layer F, as shown in Figure 3.9b. The stacking sequene becomes $ABCDEFA|FABCDE$..., where | indicates the plane on which slip occurs. The result is an intristic stacking fault, and the same sequence can be obtained if four layers (BCDE) were removed. This result is analogous to the intristic stacking fault $..ABC|BCA...$ in fcc metals, that can also be obtained by either slip ir removing an atomic layer.

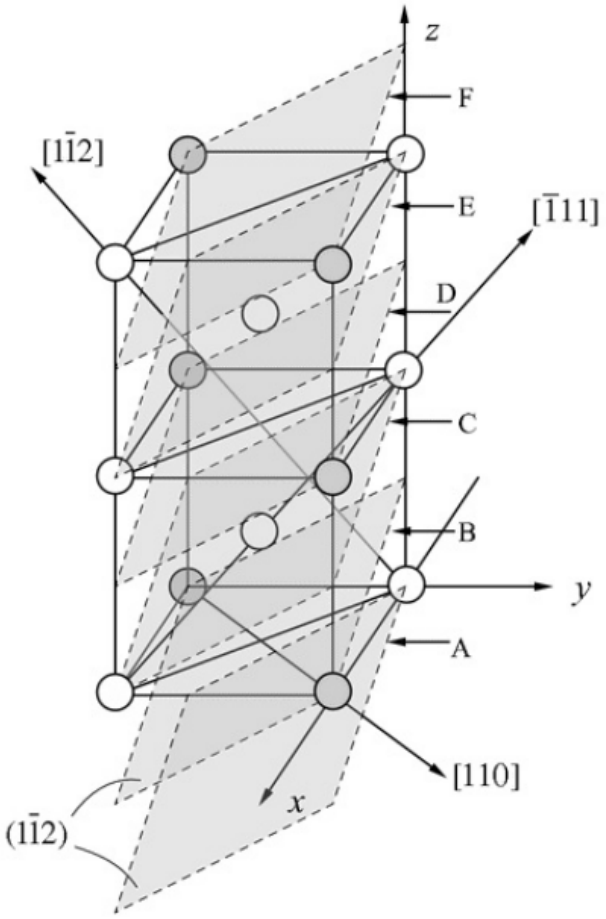

Figure 3.8: The (1$\bar{1}$2) planes of a bcc crystal showing the six layers comprising the ABCDEF... stacking sequence. [19]

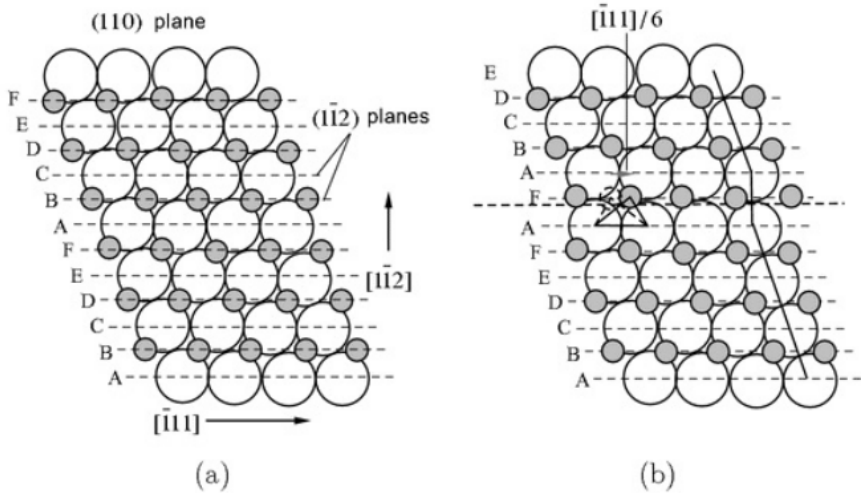

Figure 3.9: BCC crystal viewed along the [110] direction, showing the stacking sequence on the (1$\bar{1}$2) plane (a) Perfect stacking sequence ABCDEF... (b) If the layer slips relative to layer A by $\frac{a}{6}[\bar{1}11]$, it becomes layer Fcreating an intristic stacking fault [19]

Chapter 4

Molecular dynamics

4.1 Why simulations

Computer simulation is a widely used tool in modelling natural systems and predicting dynamic behavior in many scientific fields, both in academic research and industry. It allows for adequately describing structure, energetics and dynamics at the microscopic level, which govern material properties on the macroscopic level. Therefore it provides convenient access to material properties, particularly if they are difficult to obtain by experiment, like in the scope of this thesis where elastic properties of dislocations are under study. It is achieved through numerical solutions to problems, where analytical solutions are impossible, such as the many-body problem, and permits the prediction of the system under a set of parameters and initial conditions. Furthemore, simulation technique is also a useful tool for toxic, explosive or in any other way hazardous substances for which more detailed information is available from calculations of this type than it is ever possible to get from real experiments.

Over the years several simulation techniques have developed both classical, where Newton's equations of motions is solved, and quantum for which the Schroedinger's equation is solved. Regarding the classical ones, most widely used are Molecular dynamics (MD) and Monte Carlo (MC) methods. In the Monte Carlo calculation, the positions of particles are randomly sampled and averaged. For this reason, only the equilibrium properties can be calculated, whereas Molecular Dynamics was originally designed for relaxation phenomena and to study transport propertis in general.

Alder and Wainright first introduced Molecular Dynamics (MD) simulations in 1957, who studied several hunderd interacting hard-sphere particles. Their efforts delivered quantitive properties regarding the behaviour of simple liquids. [20, 21] The first simulations on dislocations began few years later in 1960s. The

papers published, especially the classic ones by Vitek and Duesbery [18], have identified many of the peculiar characteristics of dislocation behavior in bcc metals and have laid the groundwork of current investigations.

Multiscale materials modeling of mechanical properties such as crystal plasticity and strength requires an in depth understanding of fundamental defects and deformation processes.
Dislocation and their dynamics are well known and associated with deformation and plasticity. The predictive atomic scale modeling of solids with dislocations provides an insight into relevant aspects regarding elasticity, including elastic moduli and how the presence of dislocations affect these moduli. Also, the single-crystal elastic moduli often serve as basic constraints on interatomic potential used in the atomistic simulation of dislocations and other defects. [22]

4.2 Molecular Dynamics

A model for molecular dynamics contains in general two contributions: one that describes the interaction between the molecules of the system and a second that describes the interaction between molecules and their environment. The first contribution is actually the function of the potential model. This means that this function describes(even indirectly) the shape of these molecules or better their electronic distribution. In fact, the potential function is defined, the symmetry of the molecules, their elasticity etc are determined. For simplicity, we assume only isolated systems and consequently we refer to inter-molecular interactions that depend only on the inter-molecular potential model. For an isolated system the quantity that is conserved is the total energy that is the combination of kinetic and potential energy. This quantity is, in fact, the Hamiltonian:

$$H(r^N, p^N) = \frac{1}{2m_i}\sum p_i^2 + u(r^N) = E \tag{4.1}$$

In order to find the equations of motion, we first find, the total time differential of the Hamiltonian:

$$\frac{dH}{dt} = \sum_i \frac{\partial H}{\partial p_i}\dot{p_i} + \sum_i \frac{\partial H}{\partial r_i}\dot{r_i} + \frac{\partial H}{\partial t} \tag{4.2}$$

But the Hamiltonian is time independent, thus:

$$\frac{dH}{dt} = \sum_i \frac{\partial H}{\partial p_i}\dot{p_i} + \sum_i \frac{\partial H}{\partial r_i}\dot{r_i} = 0 \tag{4.3}$$

Considering an isolated system

$$\frac{dH}{dt} = \frac{1}{m}\sum_i pi_i\dot{p_i} + \sum_i \frac{\partial U}{\partial r_i}\dot{r_i} = 0 \tag{4.4}$$

If we compare the above two equations we take:

$$\frac{\partial H}{\partial p_i} = \frac{p_i}{m} = \dot{r_i} \tag{4.5}$$

and

$$\frac{\partial H}{\partial r_i} = \frac{\partial U}{\partial r_i} \tag{4.6}$$

And by subistitution we take

$$\sum_i \dot{r_i}\dot{p_i} + \sum_i \frac{\partial H}{\partial r_i}\dot{r_i} = 0 \tag{4.7}$$

$$\sum_i (\dot{p_i} + \sum_i \frac{\partial H}{\partial r_i})\dot{r_i} = 0 \tag{4.8}$$

Due to the fact that velocities are independent from each other, the last equation is satisfied only when for each atom/molecule i :

$$\frac{\partial H}{\partial r_i} = -\dot{p_i} \tag{4.9}$$

Equations (4.6) and (4.7) are the Hamiltonian equations of motion. For a system of N spherical molecules, these equations correspond to a system of 6N first order differential equations which are equivalent to 3N second order differential equations of Newton. If we eliminate the momentum fro Hamiltonians equations, we take:

$$\frac{\partial H}{\partial r_i} = -m\ddot{r_i} \tag{4.10}$$

And by using the relation

$$\frac{\partial H}{\partial r_i} = \frac{\partial U}{\partial r_i} \tag{4.11}$$

We find that

$$F_i = -\frac{\partial H}{\partial r_i} = -\frac{\partial U}{\partial r_i} \tag{4.12}$$

From the above discussion we can conclude that there is a difference between the Newtonian and the Hamiltonian dynamics. In the former, the motion is the result of the force being applied, while in the latter, forces don't appear directly, and the motion takes place in such way that the Hamiltonian is conserved. In the above discussion that system is isolated. If the system interacts with its surroundings then the Hamiltonian contains additional terms and it would not correspond to the total energy of the system, which in general in not conserved necessarily whereas Hamiltonian itself is conserved. Thus, the Hamiltonian approach is more general than the Newtonian.

4.3 Verlet algorithm

One of the most used algorithms is the central difference algorithm, that was firstly applied in MD simulationsby Verlet [23]. The mathematical derivation of the Verlet algorithm results from the Taylor expansion of the position at a preceding time $(t - \delta t)$ and a succeeding time $(t + \delta t)$

$$\vec{r}(t - \delta t) = \vec{r}(t) - \frac{d\vec{r}(t)}{dt}\delta t + \frac{1}{2}\frac{d^2\vec{r}(t)}{dt^2}\delta t^2 - \frac{1}{3!}\frac{d\vec{r}^3(t)}{dt^3}\delta t^3 + O(\delta t^4)$$

$$\vec{r}(t + \delta t) = \vec{r}(t) + \frac{d\vec{r}(t)}{dt}\delta t + \frac{1}{2}\frac{d^2\vec{r}(t)}{dt^2}\delta t^2 + \frac{1}{3!}\frac{d\vec{r}^3(t)}{dt^3}\delta t^3 + O(\delta t^4)$$

By adding in parts we obtain

$$\vec{r}(t + \delta t) = 2\vec{r}(t) - \vec{r}(t - \delta t) + \frac{d\vec{r}^2(t)}{dt^2} + O(\delta t^4) \tag{4.13}$$

Or

$$\frac{d^2 r_i(t)}{dt^2} = \frac{r_i(t + \delta t) - r_i(t - \delta t)}{2\delta t} \tag{4.14}$$

Consequently the initial differential equation $F_i = m\frac{d^2\vec{r_i}}{dt^2}$, by substituting Eq. (4.14) becomes

$$\frac{d^2 r_i}{dt^2} = \frac{r_i(t + \delta t) - 2r_i(t) + r_i(t - \delta t)}{\delta t^2} = \frac{F_i(t)}{m} \tag{4.15}$$

All above differential equations are solved numerically. The crystallographic positions of the chosen crystal strucure are the initial positions of the simulation, and the initial velocities are chosen from the Maxwell-Boltzmann distribution corresponding to a temperature T of choice. These initial positions and velocities consist the initial conditions to the numerical problem.

4.4 Interatomic potential - TBSMA

The interatomic interactions are determined from the potential. In this work, a semi-empirical potential is used and it is an analogy to the theory of Tight Binding scheme in the Second Moment Approximation (TBSMA). The interaction energy in copper derived from a phenomenological N-body potential according to which the energy of an atom i in the crystal is expressed by [27]

$$E_i = \sum_{j \neq i} A e^{-p(\frac{r_{ij}}{r_0} - 1)} - \sqrt{\sum_{j \neq i} \xi^2 e^{-2q(\frac{r_{ij}}{r_0} - 1)}}) \tag{4.16}$$

Table 4.1: Parameters of TBSMA potential model for Al and Cu.

el/ment	r_0	A (eV)	ξ	q	p	C_1	S_1	C_2
Cu	3.6015	1.675288×10^{-3}	0.505	2.2	13.5			
Al	4.02	0.178	1.3831	2.07	6.50	0.00947	0.00515	0.01664

In the above expression, the first term is a short-range repulsive term described as a sum of Born-Mayer ion-ion repulsions and denotes the pair-wise repulsive energy terms. [24] The second term is attractive and denotes the many-body metallic bonding potential that is obtained by intergrating the local density of states up the Fermi level [34]. The free parameter p is associated with the bulk modulus. The distance r_{ij} is the distance of atom at site i from atom at site j and r_0 denotes the first neighbor distance. For face-centered cubic lattices, it is $r_0 = \frac{\alpha_0}{\sqrt{2}}$, where α_0 is the corresponding lattice constant at T=0K. The parameter q represents the distance dependence of the hoping intergrals between atoms at site i and atoms at site j, ξ is an effective hopping intergral.

The parameters A, p, q, ξ and r_0 in general are adjusted to experimental or ab initio simulation data. The selection of material properties to fit to depends on subective judgement. In the simulation of dislocations, for instance elastic constants, point defect energies stacking fault energies are physical parameters one would fit the potential function to obtain proper dislocation-related mechanical properties and better chance of describing dislocation behaviors accurately. [25].

The model used for aluminium yields the energy of an atom i as [26]

$$E_i = \sum_{j \neq i} A e^{-p(\frac{r_{ij}}{r_0}-1)} - \sqrt{\sum_{i \neq j} \xi^2 e^{-2q(\frac{r_{ij}}{r_0}-1)}}) + \sum_{j \neq i} \{[\frac{C_1 \cos(2k_f r_{ij})}{(r_{ij}/r_0)^3}] + [\frac{S_1 \sin(2k_f r_{ij})}{(r_{ij}/r_0)^4}] + [\frac{C_2 \cos(2k_f r_{ij})}{(r_{ij}/r_0)^5}]\} \tag{4.17}$$

where $\mathbf{k}_f$ stands for the Fermi wave vector of aluminum, and C_1, S_1 and C_2 are also adjustable parameters in addition to the A, p, ξ, q and r_0. Th value of the parameters of both models are listed in Table 4.1.

The potential model describing tungsten was developed by Pontikis (unpublished) with the LCAO method and is given by the Equation (4.18)

$$U_i = A_{SR} \sum_{j \neq i} (1 - \frac{r_{ij}}{\rho_{SR}}) + A_{6s}^{TF} (\sum_{j \neq i} f_d^s(r_{ij}) \rho_{6s}(r_{ij}))^{5/3} + \xi_{5d} (\sum_{j \neq i} f_d^d(r_{ij}) \rho_{5d}(r_{ij}))^{1/2} + \xi_{6s} (\sum_{j \neq i} f_d^d(r_{ij}) \rho_{6s}(r_{ij}))^{1/2} \tag{4.18}$$

where the first term corresponnds to the hard-core and is approximately zero if $r_{ij} > \rho_{SR}$. The second term is the Thomas-Fermi repulsion, the third and fourth terms correspond to the tight-binding and tight-binding-like attraction respectively. More details on the tungsten potential are given in the Appendix

4.5 Boundary conditions

In computer simulations the size of the system of molecules is usually limited by computer's memory and speed. Most of the works published are based on systems containing a few thousands to a few hundreds of thousands particles. In such small systems, the surface effect have a great impact compared to their macroscopic bulk counterparts where only a small fraction of the particles are close to the surface. In order to pass by the surface effects in MD simulations Periodic Boundary Conditions (PBC) are applied, mimicking an infinite bulk system. The use of PBC introduces identical images of the simulation box on each of the box as shown in Figure 4.1 .

Consequently, a particle that leaves the simulation box during the run re-enters it through the opposite site of the same direction with the same velocity. The particles near the borders can interact with the adjacent copy, in this way the undesired surface effect can be avoided. One should notice that the simulation box has to be still long enough so that particles do not interact with themselves. An convention is to use at least two times the cut-off radius of the potential as the box length.

The simulation of dislocations need special care in the way the boundary conditions are imposed. First, a

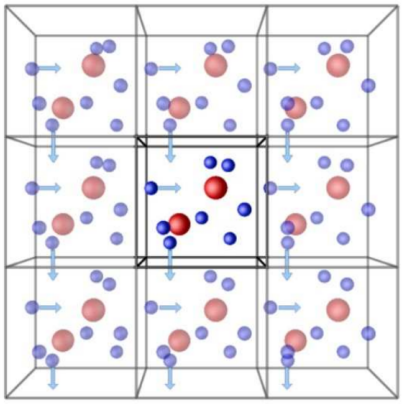

Figure 4.1: Periodic Boundary Conditions. Images of the simulation box (in the centre) are attached side by side in all dimensions. When a particle leaves the box from one side, it re-enters from the opposite one with the same velocity. [28]

dislocation creates a long-range elastic field which needs to be taken into account. Second, it is impossible to include a single dislocation is a simulation box with full periodic boundary conditions: the dislocation opens a displacement discontinuity and another defect is needed to close the discontinuity so that the total Burgers vector would be zero.[22] Thus, in our approach we use PBC along the dislocation line while along the other directions, i.e. x,y directions, Helicoidal Boundary Conditions (HBC) are imposed. HBC are a variation of the PBC. [29] In practice, when an atom leaves from one side of the box, it returns back to its previous position but shifted in z-direction and then it enters from the other opposite site as supposed to. A

visualization of the HBC conitions is shown in Figure 4.2

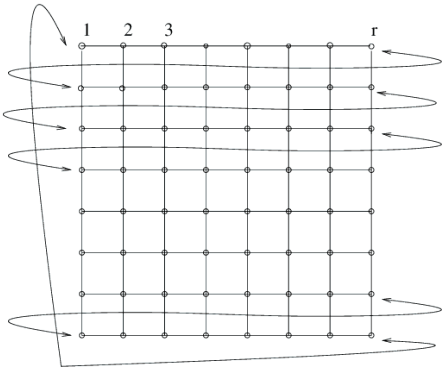

Figure 4.2: Two dimensional lattice with helicoidal boundary conditions. [30]

4.6 Statistical ensembles. Thermostat and Barostat

MD simulations can be realized in several statistical ensembles. In the microcanonical ensemble (NVE) the number of particles N of an isolated system with constant volume V have a total energy E_T being constant. The Hamiltonian of the system coincides with the total energy and can be expressed as:

$$H = E_T = K + U = \sum_i \frac{p_i^2}{2m_i} + \sum_i U_i$$

where K and U correspond to the kinetic potential energy of the system respectively, p_i is the momentum of the i_th atom, and U_i is the potential energy of the atom. In order to imitate the canonical ensemble NVT, a thermostat is commonly used. Thus, to control the temperature, an additional degree of freedom s, and its associated momentum p_s is introduced, to account for a virtual thermal bath [31], which has been proved its Hamiltonian refers to the canonical distributon. [32]. The Hamiltonian of the system then become:

$$H = \sum_i^N \frac{p_i^2}{2m_i s^2} + \sum_i^N U_i + \frac{p_s^2}{2Q} + (3N+1)k_b T ln s \tag{4.19}$$

where Q is an effective mass of the thermostat that determines the frequency of the temperature fluctuations, k_B is the Boltzmann's constant and T is the temperature of the thermal bath.

If the pressure of the system needs to be controled, a barostat is applied. The barostat adds new terms in the Hamiltonian, in a similar way as the thermostat, although in this case, the fluctuation of the box is allowed so that the pressure can match the external pressure. The barostat used in this thesis was the Andersen barostat [33]. When the thermostat and the barostat are combined, the temperature and the pressure are kept constant corresponding to the Isothermal-Isobaric ensemble (NPT). In that case, the Hamiltonian has

to following form:

$$H = \sum_{i}^{N} \frac{p_i^2}{2m_i s^2 V^{2/3}} + \sum_{i}^{N} U_i + \frac{p_s^2}{2Q} + (3N+1)k_B T ln s + \frac{p_V^2}{2W} + P_{ext}V \tag{4.20}$$

where V is the volume of the system and W is the effective mass of the Andersen piston as Q is the effective mass of the Nose thermostat. In this case, the equations of motion become:

$$\frac{\partial^2 \vec{r_i}}{\partial t'^2} = -\frac{1}{mV^{2/3}} \frac{\partial U_i}{\partial \vec{r_{ij}}} - \frac{1}{s}\frac{\partial s}{\partial t'}\frac{\partial \vec{r_i}}{\partial t'} - \frac{2}{3}V\frac{\partial V}{\partial t'}\frac{\partial \vec{r_i}}{\partial t'} \tag{4.21}$$

$$\frac{\partial^2 s}{\partial t'^2} = -\frac{s}{V}V^{2/3}\sum_{i}^{N} m_i (\frac{\partial \vec{r_i}}{\partial t'})^2 - \frac{(3N+1)k_B T s}{Q} + \frac{1}{s}(\frac{\partial s}{\partial t'})^2 \tag{4.22}$$

$$\frac{\partial^2 V}{\partial t'^2} = -\frac{s^2}{3WV^{1/3}}\sum_{i}^{N} m_i (\frac{\partial \vec{r_i}}{\partial t'})^2 - \frac{s^2}{3WV} + \frac{1}{s}(\frac{\partial s}{\partial t'}\frac{\partial V}{\partial t'} + \sum_{i}^{N} \vec{r_i}\frac{\partial U_i}{\partial \vec{r_i}}) - P_{ext}\frac{s^2}{W} \tag{4.23}$$

$$\begin{aligned} \vec{r_i'} &= \vec{r_i} V^{1/3} \\ t' &= \int^t \frac{\partial t}{s} \end{aligned} \tag{4.24}$$

Chapter 5

Method-Computational details

5.1 Computational details

We aimed to calculate the elastic constant C_{44} and stacking fault energy from the properties and behavior of screw dislocations in aluminum (fcc), copper (fcc) and tungsten (bcc). For the aluminium and copper the computational box with X,Y and Z directions parallel to the [111], [11$\bar{2}$] and [1$\bar{1}$0] directions are generated by repeating this cell in the three space directions. The simulation boxes for the case of aluminum consist of $11 \times 8 \times 8$ and $20 \times 28 \times 8$ cells with 6720 and 26880 atoms respectively. The lengths of the boxes are approximately $(70, 69, 23)$ Å and $(139, 138, 23)$ Å. For the case of copper the simulation box contains $25 \times 35 \times 8$ cells with 42000 atoms. The lengths of the box in the three directions are $(156, 154, 20)$ Å.

A perfect screw dislocation line oriented along Z direction and with Burgers vector $b = \frac{1}{2}[1\bar{1}0] = \alpha/\sqrt{2}$ is introduced at the center of the simulation box ($X = 0, Y = 0$). For both fcc crystals, Al and Cu, the systems were equilibrated to 0K using quenched molecular dynamics with periodic boundary conditions along Z direction and helicoidal boundary conditions along x and y directions of the simulation box. Also, a screw dislocation was introduced and were equilibrated at 400K to check its stability in the crystal at a finite temperature.

The model parameters for Al of the potential [26] used are $C' = 27.8$ GPa, $C_{44} = 29.618$ GPa, the anisotropy factor A=1.0654 and stacking fault energy $\gamma \approx 136 mJ/m^2$. The lattice constant for aluminum is $\alpha = 4.02$Å. For Cu the model [27] parameters are $C' = 23.7$ GPa, $C_{44} = 72.8$ GPa, A=3.07, $\alpha = 3.6015$ Å and $\gamma 45 mJ/m^2$.

In the case of tungsten, the X,Y and direction are parallel to [1$\bar{1}$0, [11$\bar{2}$] and [111]. The simulation box consists of $18 \times 10 \times 14$ cells containing 15120 atoms. The screw dislocation parallel to Z direction of Burgers vector $b = \frac{1}{2}[111] = \alpha\sqrt{3}/2$ is introduced similarly at the centre of the simulation box (X=0,Y=0). The

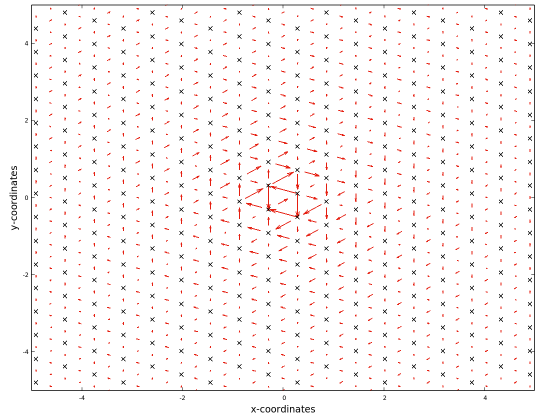

Figure 5.1: DDM of the screw dislocation before damping (Al 6720 atoms)

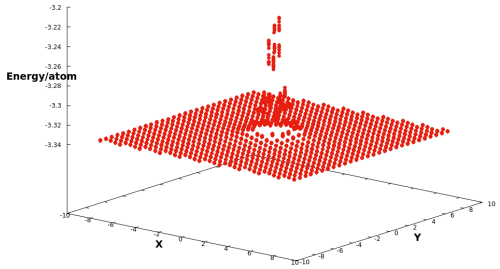

Figure 5.2: Energy per atom in x-y plane around a perfect screw dislocation at 0K (Al 6720 atoms)

potential for tungsten [to be published] have $C' = 160.86$ GPa, $C_{44} = 161.72$ GPa, $A \approx 1$ and $\alpha = 3.158$ Å.

Dislocation representation

To visulaize the dislocation, we plot the differential displacement maps (DDM) of the screw dislocation.[34] Each point represents a column of atoms. The dislocation line and Burgers vector are parallel to the atom columns, i.e. along z direction (out of plane). The DDM map is constructed by first computing the atom displacement along z direction its respect to perfect lattice for each column. The arrows then indicate the difference between displacements of neighbouring columns. The length of the arrow is proportional to the magnitude of displacement difference and the direction of the arrow indicate the sign of the displacement diffrence, i.e. the column that the arrow points to has a larger displacement than the column on the other end of the arrow. Because the lattice is periodic in z direction. The displacement difference between any two columns can be only defined *modulo* b.

5.2 Results

5.2.1 Aluminium (fcc)

6720 atoms

The displcacement map of the dislocation before damping is shown in Figure 5.1 and the site energies in x-y plane is shown is Figure 5.2 depicting the major role of helicoidal boundary conditions as no borders are shown at the edges of the box.

We started with the accurate determination of the dislocation position. Before the relaxtion of the system a {111} plane normal to x-direction was chosen. Plotting z ($[1\bar{1}0]$) positions along y ($[11\bar{2}]$), z=f(y) yields

discrete sigmoidal graphs corresponding to $u = (b/2\pi)\arctan(z/y)$, in Figure 5.3 is depicted one of them for z between 9.8 and 11.4 Å. Fitting a function of the form $f(x) = a * arctan((x - x_0)/b) + c$ on the data points results in $f(x) = 0.452\arctan(x/1.124) + 10.66$.

The value of the Burgers vector is found b= $0.452 \times 2 \times \pi = 2.84$ Å in agreement with the elastic prediction.

The derivative of these functions are Lorentzians with the maximum located at the effective position of the dislocation. The parameters found from the fitting to the displacement data points were used to evaluate the analytical form of the derivative that is shown in Figure 5.4. The dislocation is centered at $(X = 0, Y = 0)$.

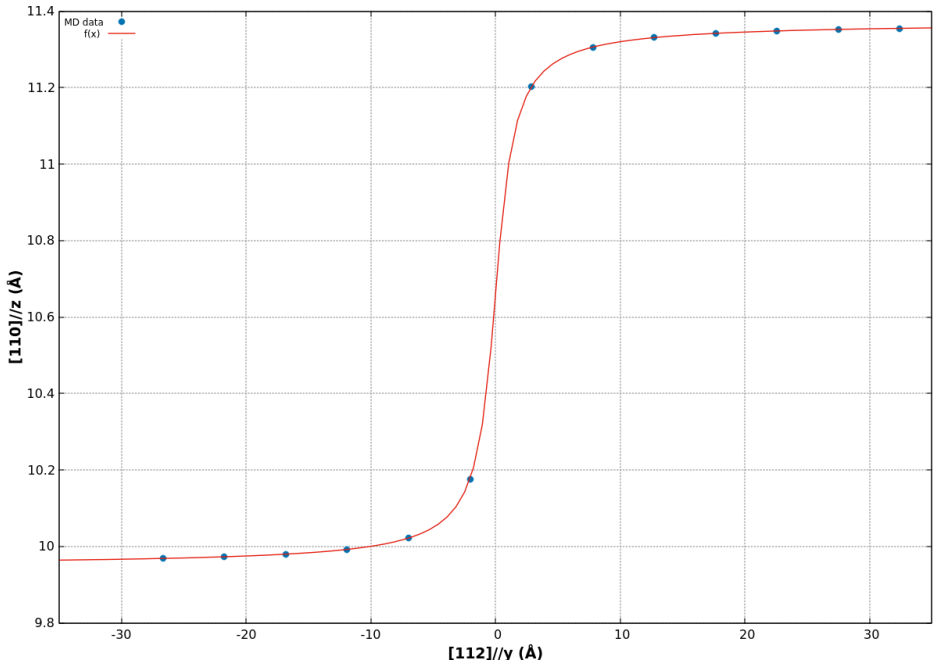

Figure 5.3: z coordinate as function of y on {111} plane after the screw dislocation was introduced (Al 6720 atoms)

The strain energy due to dislocation is found the following way: the total energy in excess of cylinders centered at (0,0) with the dislocation is subtracted from the total energy of cylinders in a perfect crystal. We only consider cylinders of radius r greater than $r_0 \approx 3$ Å and exclude atoms with positions $r = \sqrt{x^2 + y^2} < r_0$, so that the energy of the core is not included because linear elasticity fails at the core of the dislocation. In Figure 5.5 is shown the elastic strain energy in a cylindrical shell of increasing outer radius R and a constant inner radius r_0 with its axis at (0,0). The logarithmic dependence on distance of the elastic strain energy is described by Eq. (2.7). From the data the slope is found a=2.643 (eV), therefore shear modulus can be calculated directly from Eq. (3.7).

$$\frac{Gb^2}{4\pi} = \frac{a}{L} \Rightarrow G = \frac{4 \times \pi \times 2.643eV}{(2.84)^2 \times 22.74\mathring{A}^3} \Rightarrow G = 0.181eV/\mathring{A}^3$$

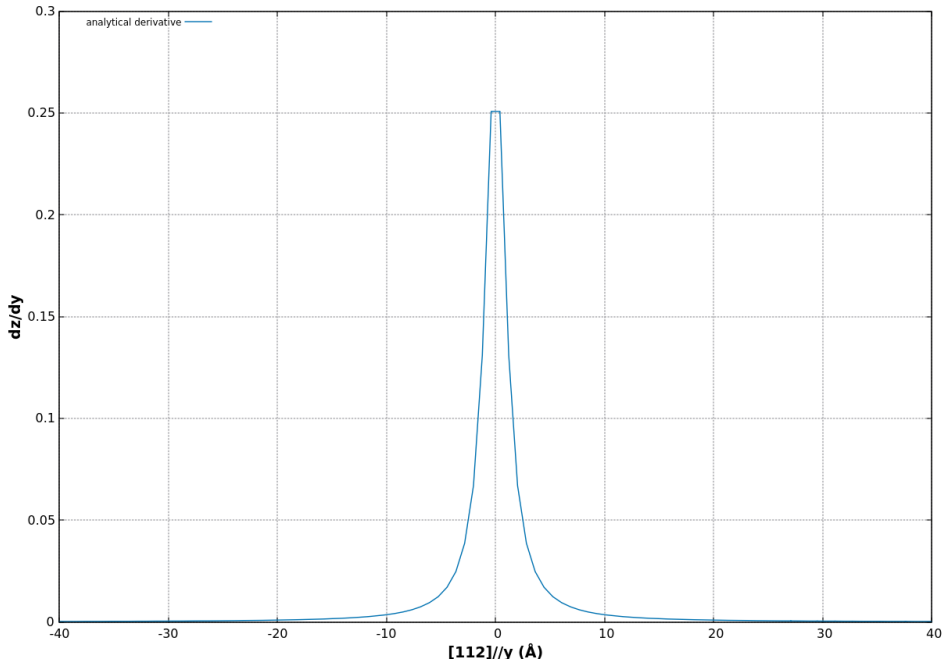

Figure 5.4: Analytical derivative of z=f(y) indicates the position of an $\frac{1}{2}[1\bar{1}0]$ screw dislocation (Al 6720 atoms)

or

$$G = 28.97GPa$$

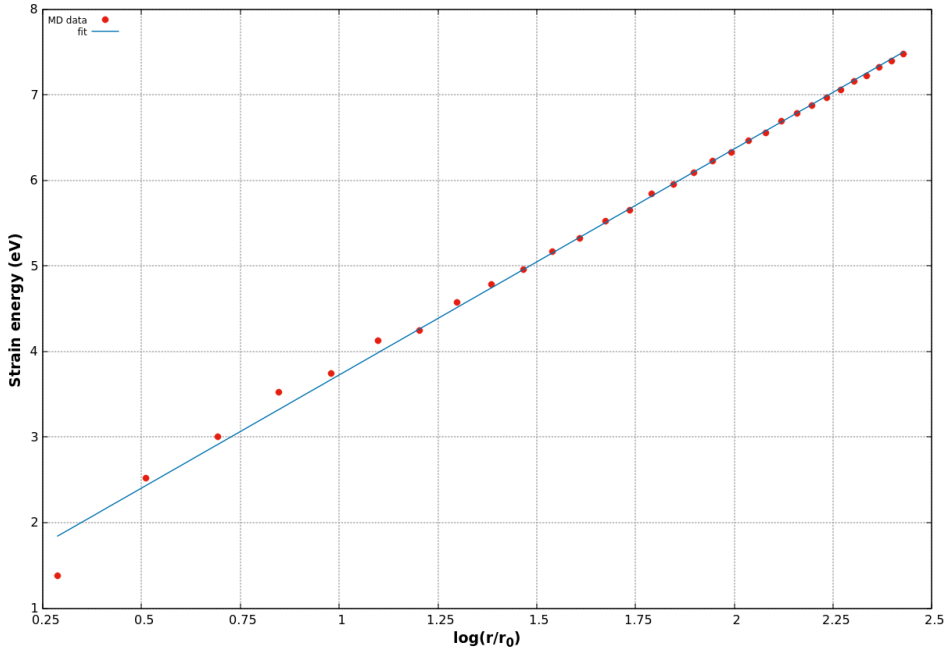

Figure 5.5: The strain energy within a cylinder of radius R that contains a screw dislocation along its axis (Al 6720 atoms)

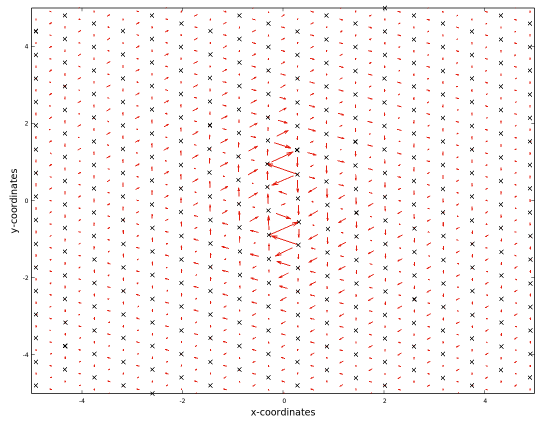

Figure 5.6: DDM of the dissociated screw dislocation after damping at 0K (Al 6720 atoms)

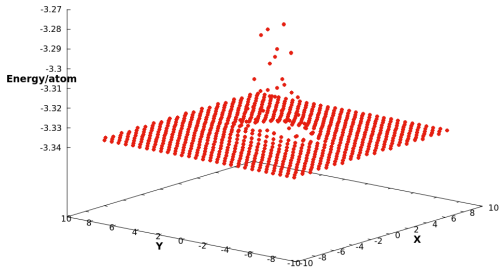

Figure 5.7: Site energies in x-y plane around a dissociated screw dislocation at 0K (Al 6720 atoms)

For isotropic cubic crystals shear modulus equals to the elastic constant C_{44}, though for anisotropic media that is not the case. A correction can be taken into account to calculate elastic constant C_{44} more precisely. We multiply shear modulus G with the square root of anisotropy factor. Therefore

$$C_{44} = G \times \sqrt{A} = 28.97 \times \sqrt{1.065395} = 29.9GPa$$

In Figure 5.6 we see the DDM of the disssociated screw dislocation, the two Shockley partials are shifted along $[11\bar{2}]$, and in Figure 5.7 is the energy per atom of the dissociated dislocation at x-y plane.

After the damping the screw dislocation with Burgers vector $\vec{b} = \frac{1}{2}[1\bar{1}0]$ dissociates into Shockley partials bounded by a $\{111\}$ stacking fault ribbon. The discrete graphs are then described by the sum of two Lorentzians shifted along $[11\bar{2}]$ and the derivatives do contain two maxima as shown in Figure 5.8 and in Figure 5.9. Fitting of the function $f(x) = a\arctan((x - x_1)/b) + a\arctan((x - x_2)/b) + c$ gives the following values for the parameters

$$a = 0.231, x_1 = 2.71305, x_2 = -2.34849, b = 1.8405, c = -3.556$$

The dissociation width between the two partial dislocations is then $r_{eq} = |x_1 - x_2| = 5.062$ Å. Shockley partials have equal Burgers vectors and each is inclined 30° to the initial Burgers vector and 60° to each other. The norm of the partial Burgers vector is $b_2 = b_3 = \frac{1}{6}[112] = \frac{\alpha}{\sqrt{6}}cos(30) = 1.42$ Å.
As for the case of one perfect dislocation, we can estimate the partial Burgers vector in the relaxed configuration. From the parameters fitted to the graph in Figure 5.8, it follows

$$b_p = 0.231 \times 2 \times \pi = 1.45\mathring{A}$$

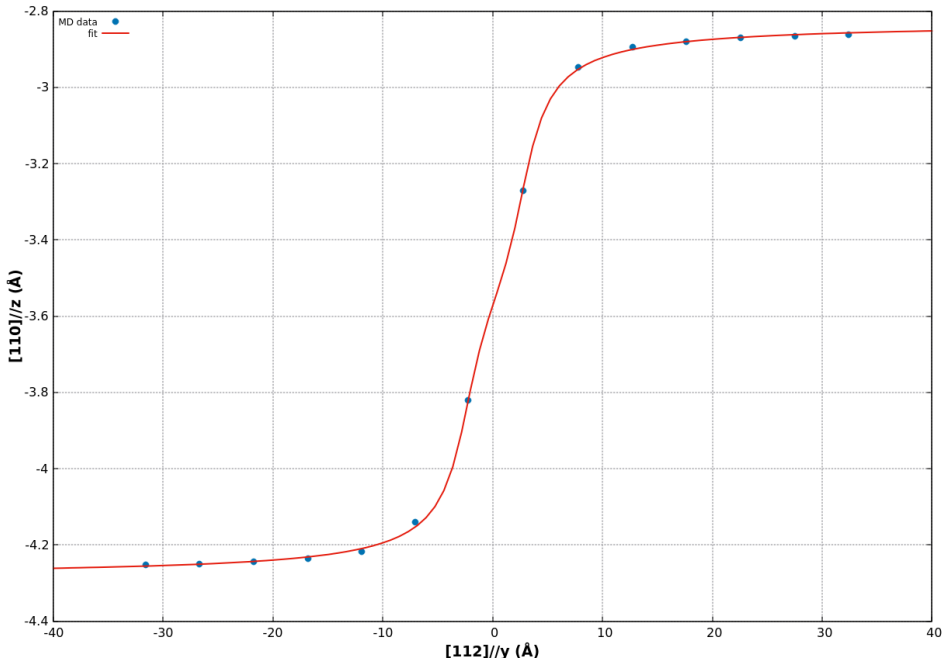

Figure 5.8: z coordinate as function of y on {111} plane in the relaxed configuration of 6720 atoms

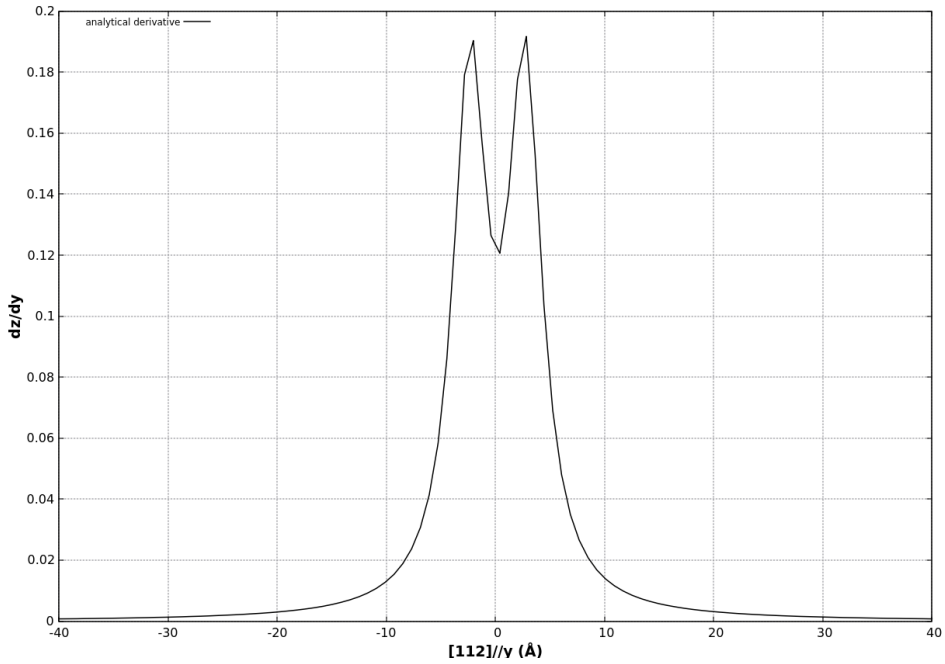

Figure 5.9: Analytical derivative of z=f(y) indicates the positions of the Shockley partials (6720 atoms)

in good agreement with the elastic prediction of 1.42 Å. Similarly in order to find the elastic energy as a function of distance we took cylindrical shells of inner radius $r_0 = 6$Å and increasing outer radius R. In the relaxed configuration the excess energy is not only due to the strain energy of partial dislocations but the sum of energy of the two Shockley partials. The interaction energy E_{12} between them and the stacking fault energy γ' are given as [35]

$$E = 2E_{partial} + E_{12} + \gamma' r_{eq} \tag{5.1}$$

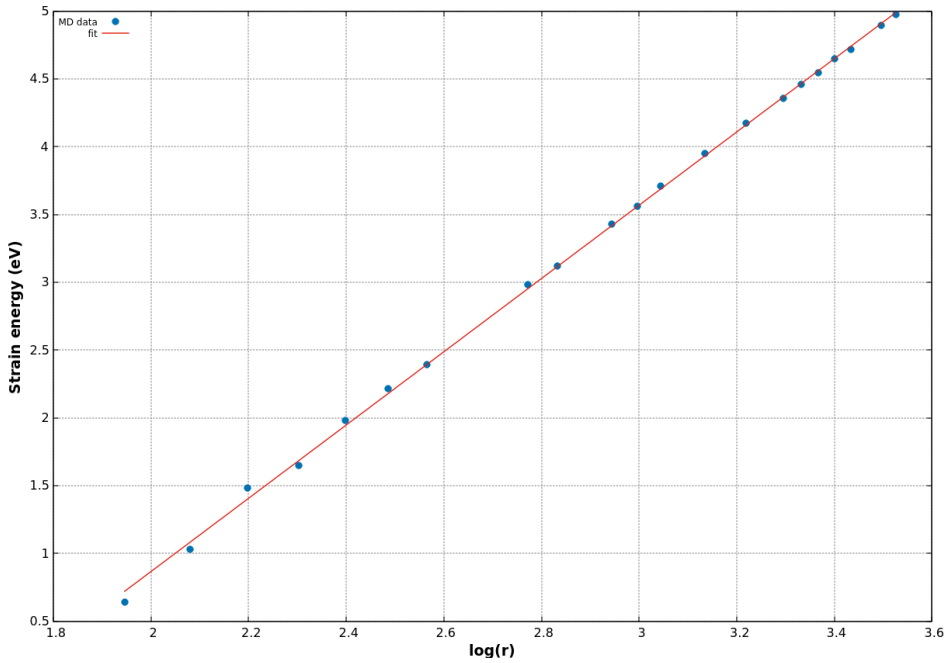

Figure 5.10: The strain energy within cylindrical shells containing two partial dislocations(6720 atoms)

$$E_{12} = (\frac{3K_3}{4} - \frac{K_1}{12} - \frac{K_2}{6})\frac{b_p^2}{4\pi} ln(R/r_{eq}) \tag{5.2}$$

$$E_{partial} = (\frac{K_1}{12} + \frac{K_2}{6} + \frac{3K_3}{4})\frac{b_p^2}{4\pi} ln(r/r_0) \tag{5.3}$$

The strain energy as a function of lnR is shown in Figure 5.10; line's gradient is a'=2.70 (eV) and the y-intercept is -4.538 (eV). Thus, from Eq. (5.1)-(5.3) the stacking fault energy equals

$$\gamma' r_{eq} - (\frac{3K_3}{4} - \frac{K_1}{12} - \frac{K_2}{6})\frac{b_p^2}{4\pi} ln(r_{eq}) - (\frac{K_1}{12} + \frac{K_2}{6} + \frac{3K_3}{4})\frac{b_p^2}{4\pi} ln(r_0) = \frac{-4.538(eV)}{22.74(\mathring{A})}$$

$$\gamma'(5.062)\mathring{A} = -0.065726eV/\mathring{A} \Rightarrow \gamma = -0.012984eV/\mathring{A}^2 \Rightarrow \gamma' = -207mJ/m^2$$

Nevertheless, from Eq. (3.7) we can calculate the effective shear modulus G' from the data in Figure 5.10.

$$\frac{G'b^2}{4\pi} = \frac{a'}{L} \Rightarrow G' = \frac{a'4\pi}{b^2 L} = \frac{2.70 \times 4 \times \pi}{2.84^2 \times 22.74} \Rightarrow = 0.185eV/\mathring{A}^3 \Rightarrow G' = 29.58GPa$$

400K

Last, we introduced the screw dislocation at 400K and then the system was equilibrated in the NVT ensemble. The dislocation before an after dissociation is seen in Figure 5.11 and Figure 5.12. As shown, the perfect screw dislocation does not vanish in a finite temperature but dissociates into partials and remains present in

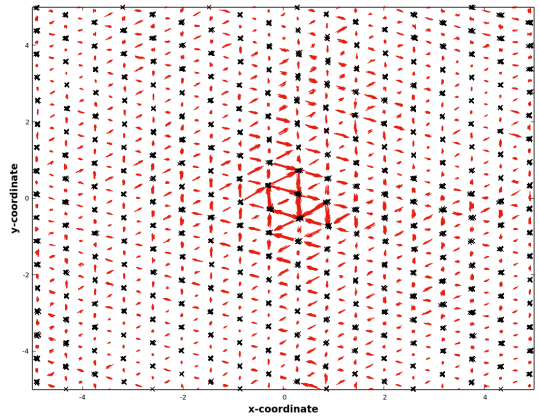

Figure 5.11: DDM of a perfect screw dislocation at 400K (Al 6720 atoms)

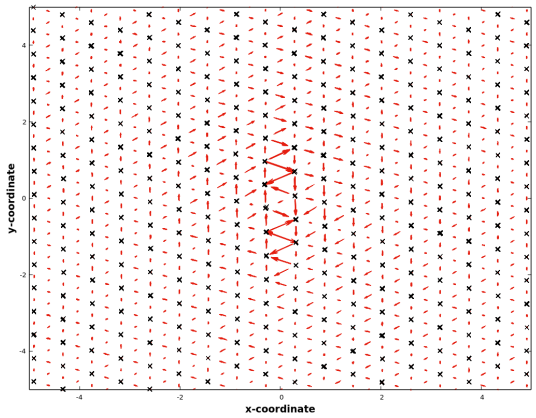

Figure 5.12: DDM of the dissociated screw dislocation at 400K (Al 6720 atoms)

the crystal.

26880 atoms

In the same fashion, elastic constant C_{44}, dissociation width r_{eq} and stacking fault energy γ' are calculated for a bigger aluminum system. The lattice vectors have the same orientation $20 \times [111]$ $28 \times [11\bar{2}]$ and $8 \times [1\bar{1}0]$, and the box lengthes are $(139.26, 137.86, 22.74168545)$Å. In Figure 5.13 is depicted the strain energy in cylindical shells of iner radius $r_0 = 3$Å and increasing outer radius R. The fitting of $f(x) = a * x + b$ to the data results in $a = 2.60689$ and y-intercept 1.14858. Therefore the shear modulus and C_{44} in this case are

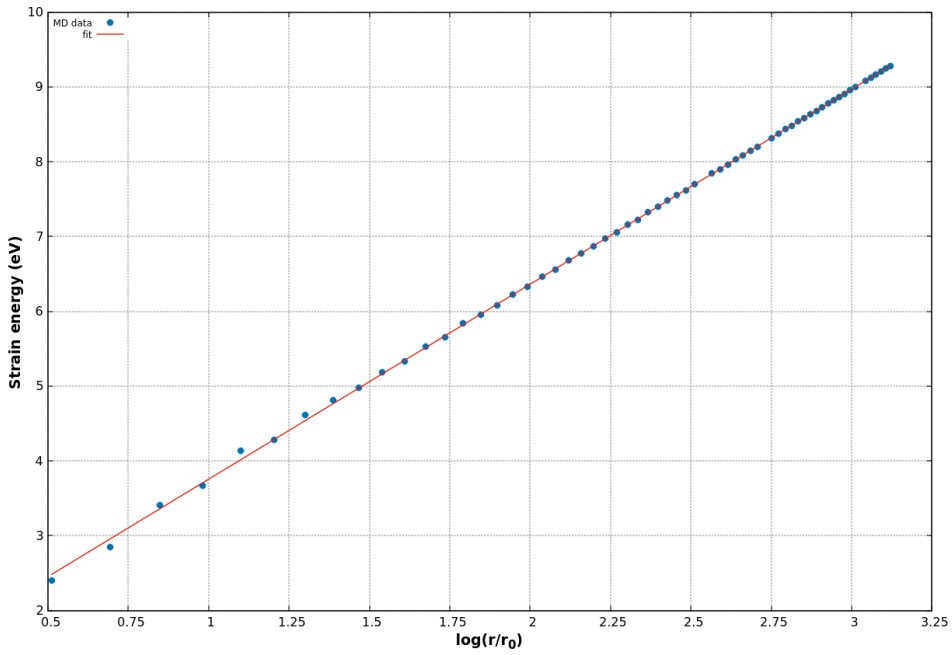

Figure 5.13: The strain energy within cylindrical shells of outter r and inner radius r_0 with a $\frac{1}{2}[1\bar{1}0]$ screw dislocation (Al 26880 atoms)

$$\frac{Gb^2}{4\pi} = \frac{a}{L} \Rightarrow G = \frac{4 \times \pi \times 2.60689eV}{(2.84)^2 \times 22.74\mathring{A}^3} \Rightarrow G = 0.178eV/\mathring{A}^3$$

or

$$G = 28.537GPa$$

and

$$C_{44} = 28.537GPa \times \sqrt{1.065395} = 29.46GPa$$

After relaxation the screw dislocation dissociates into Shockely partials; the dissociation width in this system is found from the graph of Figure 5.14, its derivative is shown in Figure 5.15. The fitting of $f(x) = a\arctan((x - x_1)/b) + a\arctan((x - x_2)/b) + c$ results in $a = 0.226, x_1 = -3.65772, x_2 = 3.91553, b = 1.23079 and c = -7.82077$, and therefore $r_{eq} = 7.57275$Å. The partial Burgers vector is

$$b_p = 0.226 \times 2 \times \pi = 1.419\mathring{A}$$

The relation of strain energy with ln(r) is shown in Figure 5.16. The slope is a'=2.67746 eV and y-intercept is -4.4704 eV. From Eq.(5.1-5.3) the stacking fault energy is estimated

$$\gamma' r_{eq} - (\frac{3K_3}{4} - \frac{K_1}{12} - \frac{K_2}{6})\frac{b_p^2}{4\pi} ln(r_{eq}) - (\frac{K_1}{12} + \frac{K_2}{6} + \frac{3K_3}{4})\frac{b_p^2}{4\pi} ln(r_0) = \frac{-4.4704eV}{22.74\mathring{A}}$$

$$\gamma'(7.573)\mathring{A} = 0.1966eV/\mathring{A} + 0.112eV/\mathring{A} + 0.00246eV/\mathring{A} \Rightarrow \gamma = -0.00803eV/\mathring{A}^2 \Rightarrow \gamma' \approx 129mJ/m^2$$

From Eq. (3.7) effective shear modulus is

$$\frac{G'b^2}{4\pi} = \frac{a'}{L} \Rightarrow G' = \frac{a'4\pi}{b^2 L} = \frac{2.67746 \times 4 \times \pi}{2.84^2 \times 22.74} \Rightarrow = 0.eV/\mathring{A}^3 \Rightarrow G' = 29.35GPa$$

5.2.2 Copper (fcc)

The above methodology of calculating the C_{44} and stacking fault energy has been applied also for the case of copper, an anisotropic material. A crystallite of 42000 atoms in a parallelepiped-shaped simulation box with fcc lattice vectors $25 \times [111] 35 \times [11\bar{2}]$ and $30 \times [1\bar{1}0]$ was used. The unit cell vectors orientation is the same as in the case of aluminum. A perfect screw dislocation with Burgers vector $\vec{b} = \frac{a}{2}[1\bar{1}0] = 2.546$ Å was introduced at the centre of the simulation box.

The displacement map of the perfect screw dislocation is shown in Figure 5.17 at 0K. The Burgers vector and the position of the perfect screw dislocation can be verified in the same way as in aluminum.

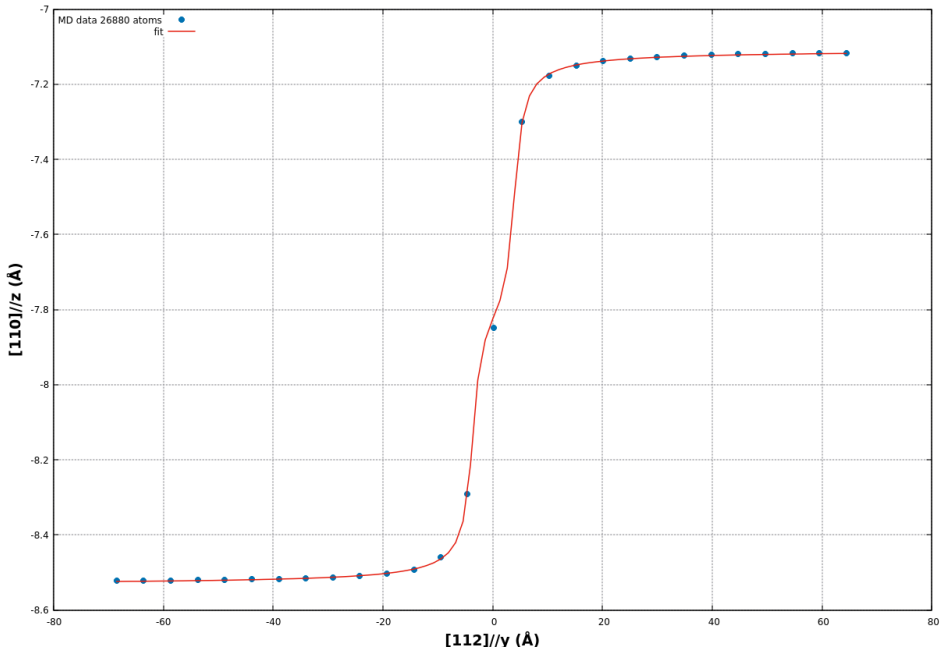

Figure 5.14: z=f(y) on a {111} plane in relaxed configuration (Al 26880 atoms)

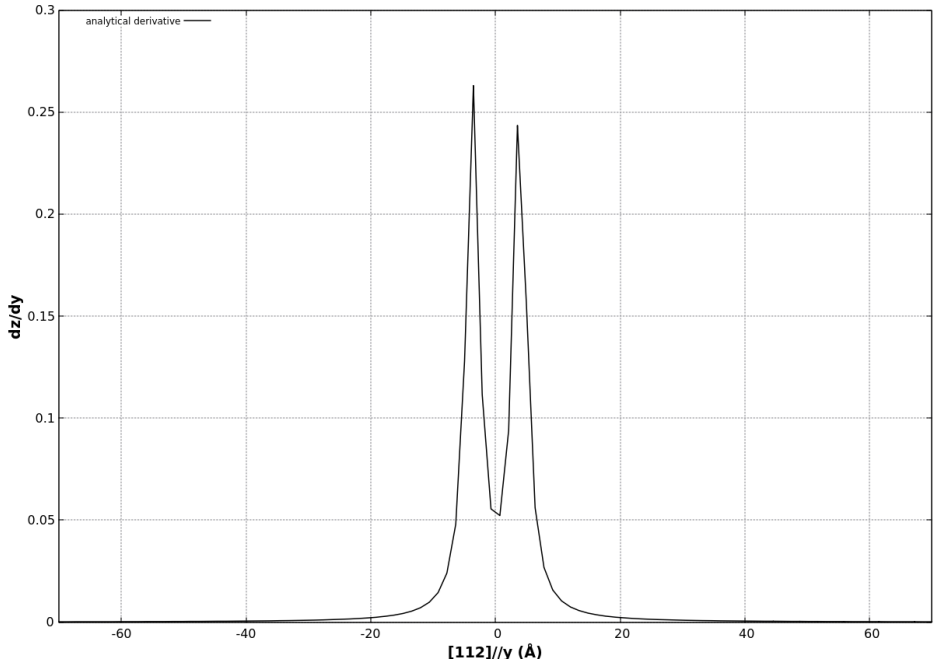

Figure 5.15: Analytical derivative of z=f(y) indicates the effective positions of the Shockley partiasl (Al 26880 atoms)

For the calculation of the shear modulus, and consequently of the C_{44}, we followed the same steps as in the fcc case. Cylindrical shells of outer radius r and inner radius r_0 were taken about the dislocation line located at the centre of the simulation box. The core radius was chosen $r_0 = 5.4$ Å. In Figure 5.19, the elastic strain energy within these cylindrical shells is shown with relation to the distance from the dislocation line. A linear fitting to the data of of Figure 5.19 yields a slope equal to 3.93162 and y-intercept equal -0.079. From Equation (3.7), we can calculate the shear modulus

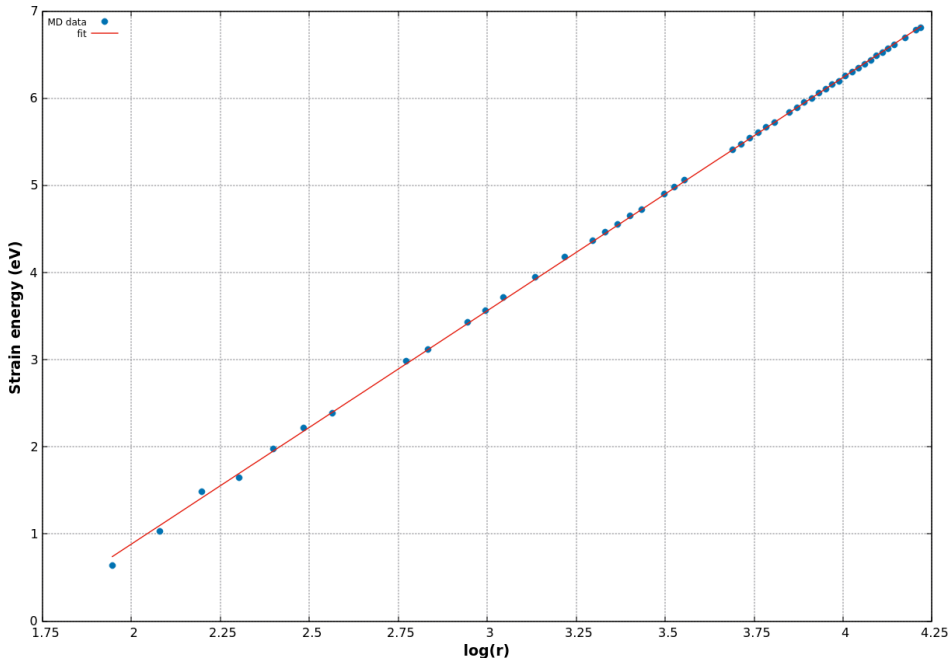

Figure 5.16: The strain energy in cylindrical shells around Shockley partials(Al 26880 atoms)

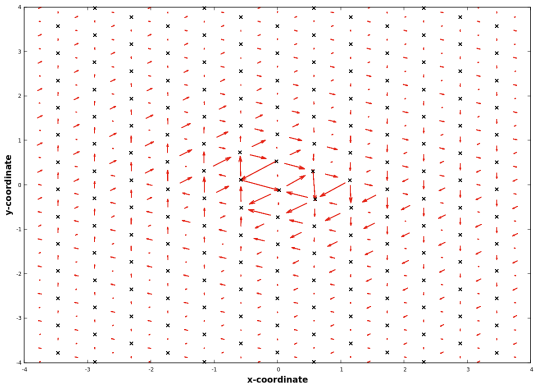

Figure 5.17: DDM around a $\frac{\alpha}{2}[110]$ screw dislocation in Cu viewed from [110] direction

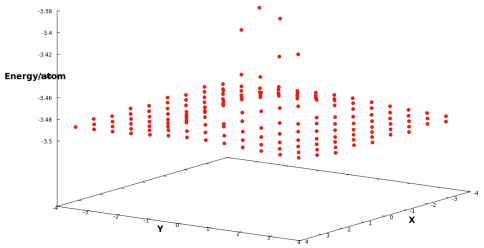

Figure 5.18: Energy per atom in x-y plane around a perfect screw dislocation at 0K in copper

$$\frac{a}{L} = \frac{Gb^2}{4\pi} \Rightarrow G = \frac{a \times 4 \times \pi}{b^2 \times L} = \frac{3.93162 \times 4 \times \pi}{2.546^2 \times 21.84} = 0.349 ev/\mathring{A}^2$$

or

$$G = 55.83 GPa$$

The mechanical behavior of copper is highly anisotropic; the elastic constants vary considerably for different crystallographic orientations. Thus, C_{44} differs from shear modulus. In this simulation model C_{44}=72.8 GPa and C'=23.70 Gpa, and anisotropy ratio A=3.0717. Thus, the C_{44} will be:

$$C_{44} = G \times \sqrt{A} = 55.83 \times \sqrt{3.0717} = 97.85 GPa$$

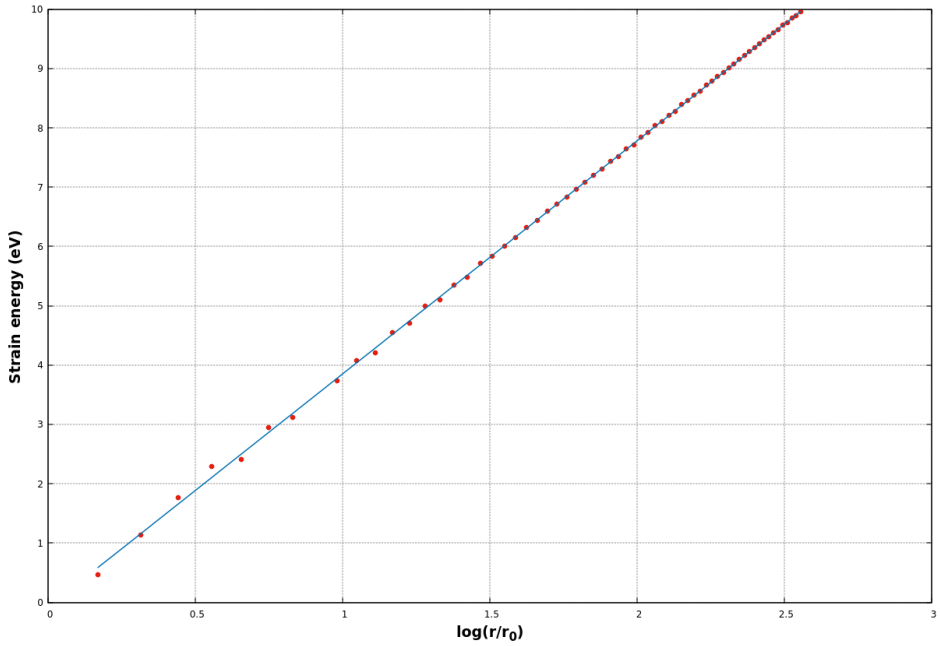

Figure 5.19: The elastic strain energy in copper containing a $\frac{1}{2}[111]$*screwdislocation*

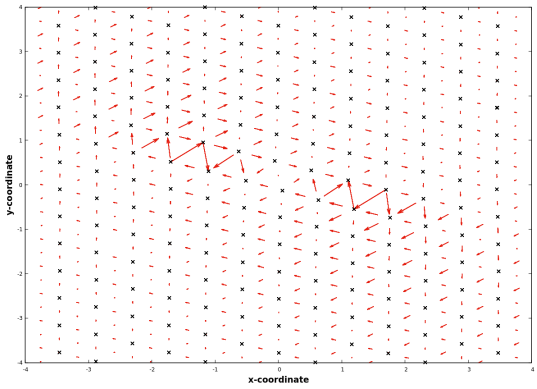

Figure 5.20: DDM of Shockely partials in Cu

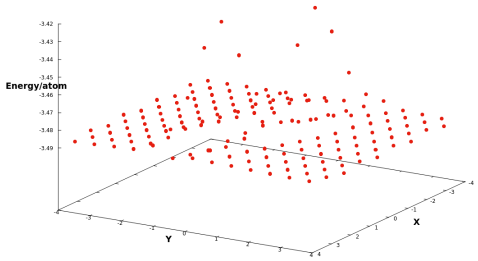

Figure 5.21: Energy per atom in Cu containing Shockley partials

After the relaxation of the system using quenched molecular dynamics, the screw dislocation has been dissociated into 30° Shockley partials. The displacement map and the energy in site are in Figure 5.20, Figure 5.21. In Figure 5.21, we can distinguish two energy maxima.

After damping of 2000 timesteps the system is at 0K. The perfect screw dislocation dissociates into Shockley partials. The dissociated dislocations are not aligned normal to the slip plane, but instead are aligned very close to 111 plane. The sigmoidal graph is shown in Figure 5.22. Because of the fact that the perfect screw dislocation in this case is not dissociated only in [112] direction, a fitting of the form $u_z = b/2\pi atan(z/y)$ in not applicable. Instead, Spline interpolation to the data was used in order to derive its numerical derivative that is shown in in Figure 5.23. The two maxima indicate the positions of the Shockley partials. The

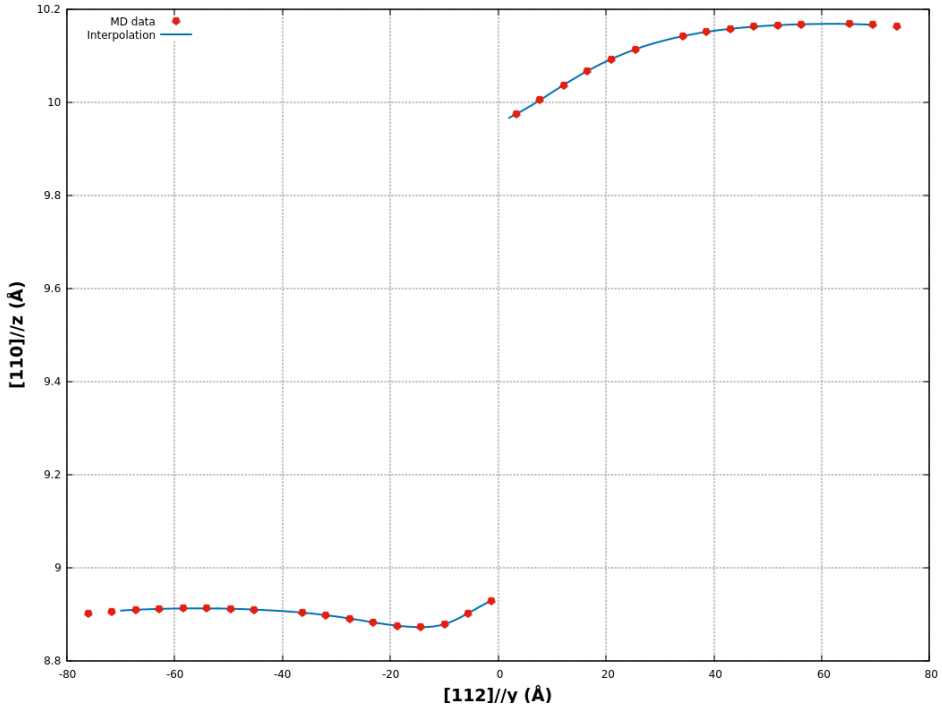

Figure 5.22: z=f(y) viewed from [111] direction in Cu with Shockley partials

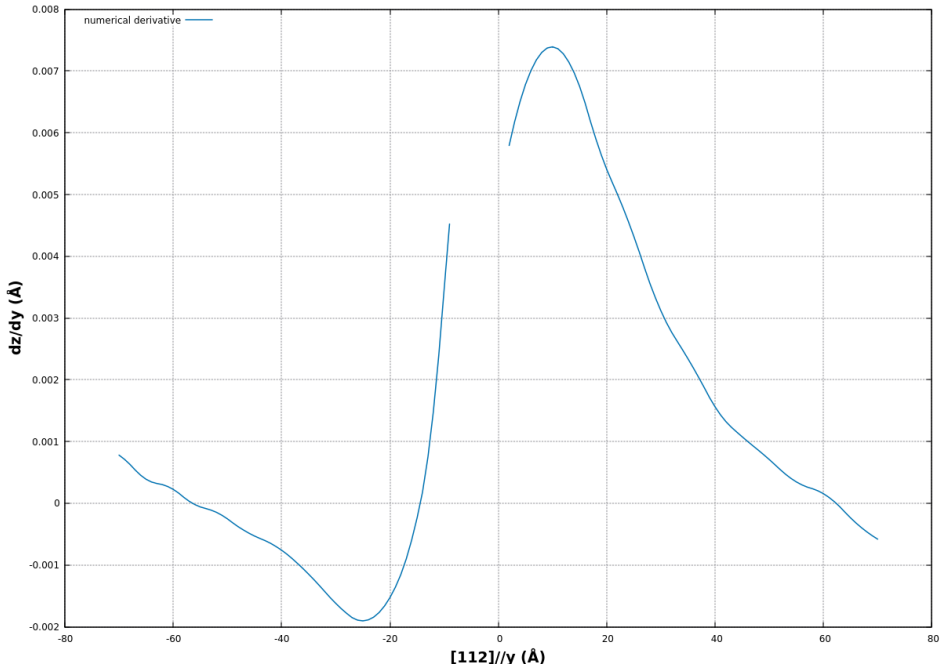

Figure 5.23: Numerical derivative of z=f(y) indicates the effective positions of the Shockley partials in Cu

dissociation width is found to be r_{eq} = 34.57 Å. Similar dissociation widths between 15 Å and 45 Å have been found in another MD study of screw dislocations in Cu. [36]

To calculate the intristic stacking fault energy, we considered the elastic strain energy of the partial dislocations. The logarithmic dependence on distance of the elastic strain energy is shown in Figure 5.24.

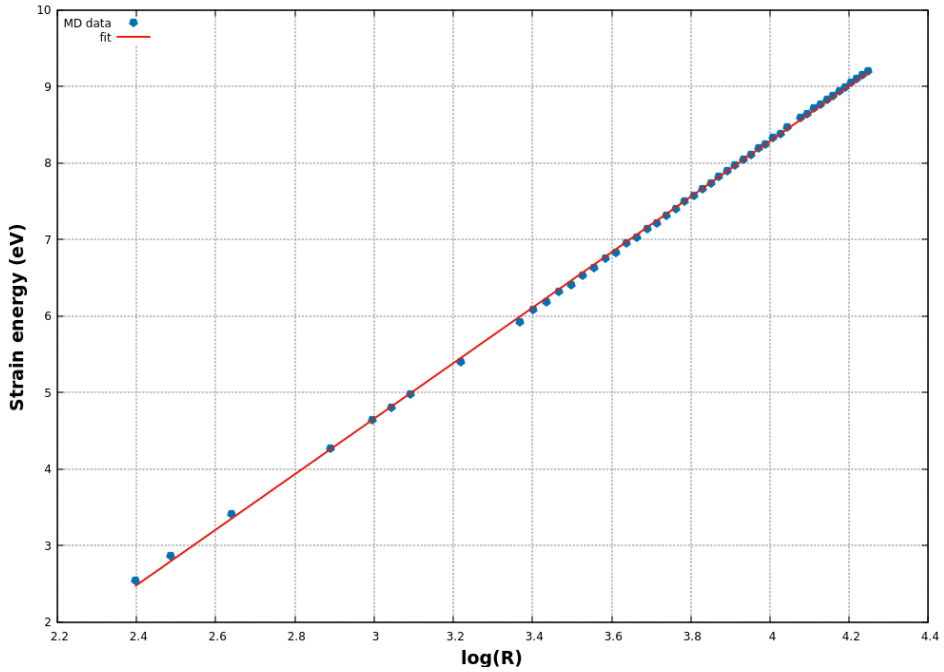

Figure 5.24: The strain energy within cylindrical shells containing Shockley partials in anisotropic copper.

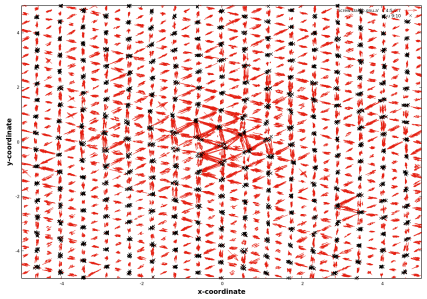

Figure 5.25: DDM of a perfect screw dislocation in copper at 400K

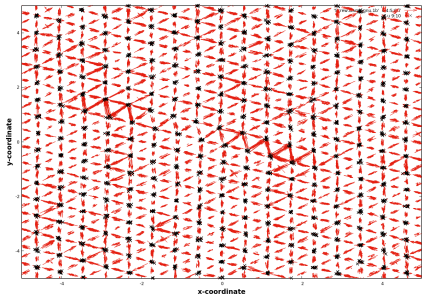

Figure 5.26: DDM of a disscociated screw dislocation in copper at 400K

The fitting of a linear function to $E \sim log(r) = a * x + b$ yields a=3.62703 and b=-6.22543.

Using the Equations (5.1-5.3), we can calculate the stacking fault energy bounded by the two partial dislocations.

$$E(r) = 3.62703log(r) - 2ln(r_0)(\frac{K_1}{12} + \frac{K_2}{6} + 3\frac{K_3}{4})\frac{b_p^2}{4\pi} - ln(r_{eq})(3\frac{K_3}{4} - \frac{K_1}{12} - \frac{K_2}{6})\frac{b_p^2}{4\pi} + \gamma' r_{eq}$$

$$\gamma' 34.57 = -6.22453eV/L + 2ln(r_0)(\frac{K_1}{12} + \frac{K_2}{6} + 3\frac{K_3}{4})\frac{b_p^2}{4\pi} + ln(r_{eq})(3\frac{K_3}{4} - \frac{K_1}{12} - \frac{K_2}{6})\frac{b_p^2}{4\pi}$$

$$\gamma' r_{eq} = 6.22453eV/21.84\mathring{A} + 0.181145eV/\mathring{A}$$

$$\gamma' = -48mJ/m^2$$

400K

The screw dislocations in an anisotropic crystals, such as copper, are stable at finite temperatures as well as in isotropic fcc crystals (Al). In Figure 5.25 and Figure 5.26, the screw dislocation is shown before and after relaxation in the (NVT) ensemble. Better visualization can be achieved with further equilibration,.The screw dislocation dissociates fairly quickly, so the system can be suffciently equilibrated containing the partial dislocations, and not the perfect dislocation.

5.2.3 Tungsten (bcc)

When the same methology was applied in a body-centered cubic metal, the resuls are satisfactory as in the case of fcc metals. The shortest lattice vector is of the type $\frac{\alpha}{2}[111]$, therefore a screw dislocation of Burgers vector $b^2 = \frac{\alpha^2}{2^2}[1^2 + 1^2 + 1^2] \Rightarrow b = 2.75\mathring{A}$ was introduced using tungsten.

The displacement map normal to dislocation line along z-axis is shown in Figure 5.27. A $(11\bar{2})$ plane was chosen in order to verify dislocation's position and Burgers vector. The fitting of the function $f(x) = a \times atan((x - x_0)/b) + c$ on the data of the discrete sigmoid graph in Figure 5.28 yields the parameters: a=0.435274, $x_0 = 6 \times 10^{-11}$, b=0.644624 and c=-1.59547. Thus,the Burgers vector $b = 0.435274 \times 2 \times \pi = 2.7349\mathring{A}$ is in total agreement with the elastic prediction. The analytical derivative of fitting function is shown in Figure 5.29.

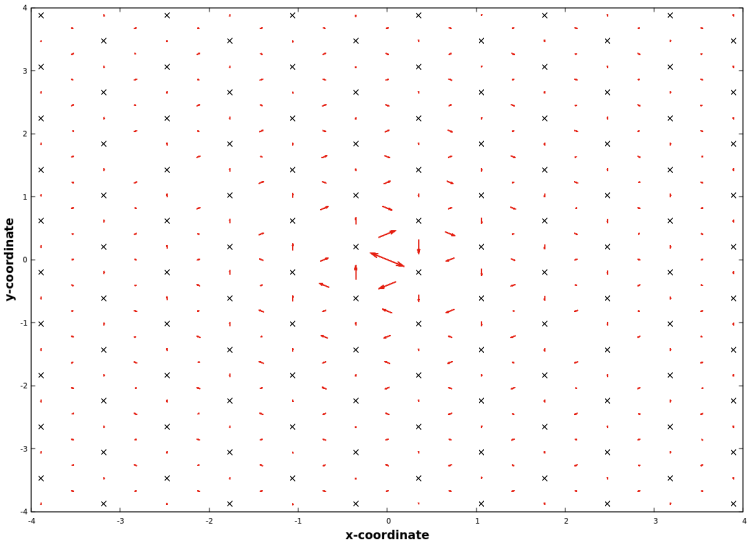

Figure 5.27: DDM of a perfect screw dislocation in Tungest (bcc) of Burgers vector $\frac{\alpha}{2}[111]$

The strain energy of the dislocation is found in the same way as in the fcc metlas; by summing the total energy of atoms contained in concentric cylindrical shells about (X,Y=0,0). The atoms in the inner core of radius taken $r_0 \approx 2b = 5.5\mathring{A}$ are excluded. In Figure 5.30 is shown the elastic strain energy in cylindrical

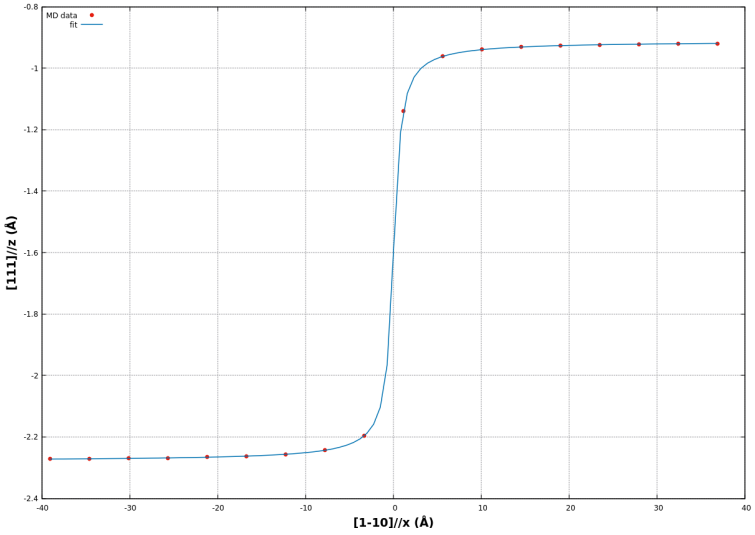

Figure 5.28: z coordinate as function of x on {111} plane before relaxation

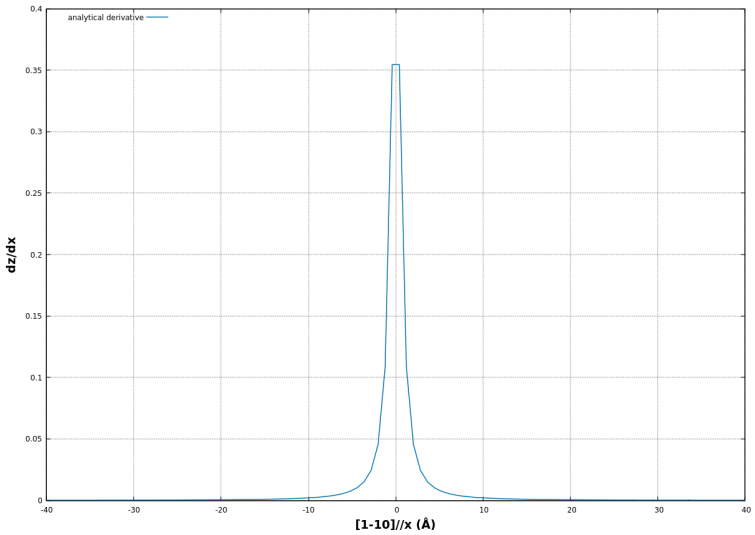

Figure 5.29: Analytical derivative of z=f(x) indicates the position of the screw dislocation in tungsten (W)

shells of an increasing outer radius r and the constant radius r_0. From the data the slope is found a=22.6016 (eV). The tungsten is fully isotropic, so the anisotropy ratio is equal to unity. The shear modulus can be calculated directly from Eq. (3.7)

$$\frac{Gb^2}{4\pi} = \frac{a}{L} \Rightarrow \frac{4 \times \pi \times 22.6016eV}{(2.735)^2} \times 38.29\mathring{A}^3 \Rightarrow G = ev/\mathring{A}^2$$

or

$$G = C_{44} = 158.65GPa$$

This value of C_{44} is in good agreement with model's parameter $C_{44} = 161.72GPa$.

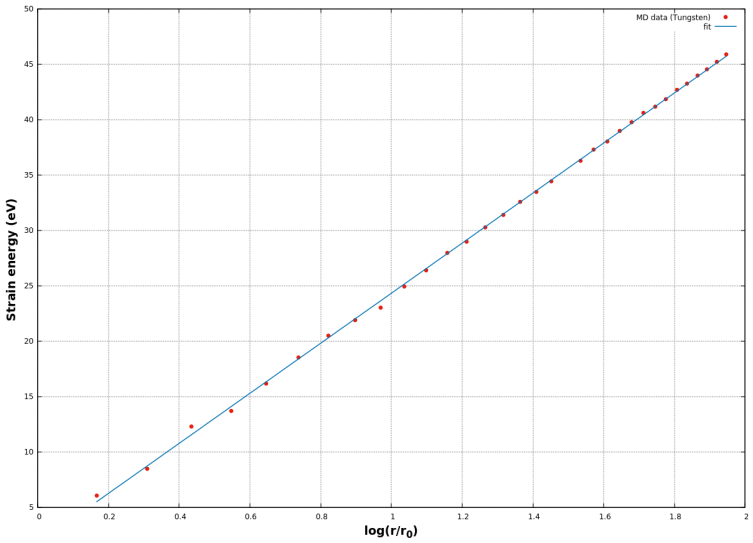

Figure 5.30: The strain energy within a cylindrical shell of inner radius r and outer radius r_0 along a screw dislocation $\frac{\alpha}{2}[111]$ in W

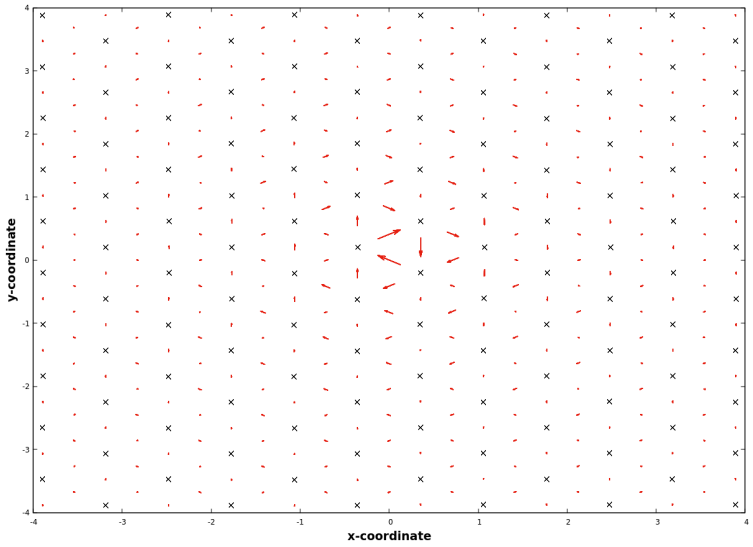

Figure 5.31: Displacement map of three partial $\frac{\alpha}{6}[111]$ screw dislocations in W

After relaxation of 2000 timesteps using quenched molecular dynamics, we obtain the configuration seen in Figure 5.31 at 0K. The perfect screw dislocation has been dissociated into three non co-planar partial dislocations. In order to find in which three planes of the same type has the perfect screw dislocation dissociated, planes normal to [110] and [112] direction were investigated to identify the partial Burgers vector.

In Figure 5.32 we see the z-coordinate as a function of y. The fitting to to the data points of $f(x) = a * atan((x - x0)/b + c$ yields a=0.145585, $x_0 = 1.9366$, b=3.09713 and c=-5.01048. The analytical derivative of this function is shown in Figure 5.33. Thus, the partial Burgers is $b_p = 0.145584 \times 2 \times \pi = 0.915$ Å that

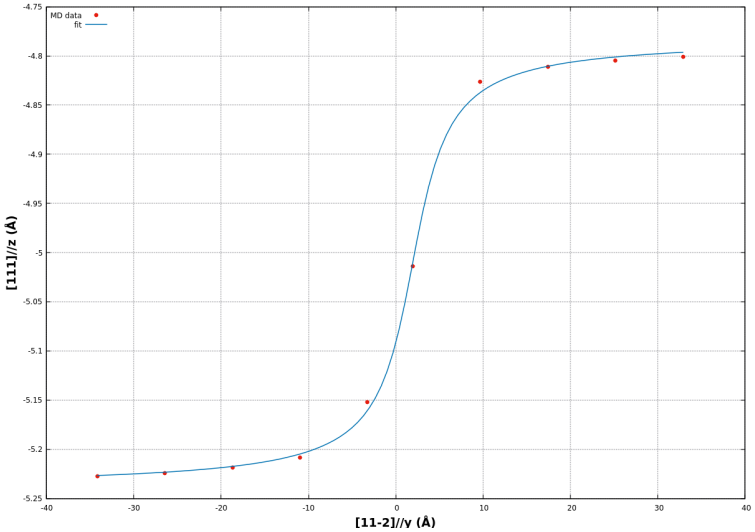

Figure 5.32: z=f(y) in tungsten (W) viewed from [110] direction.

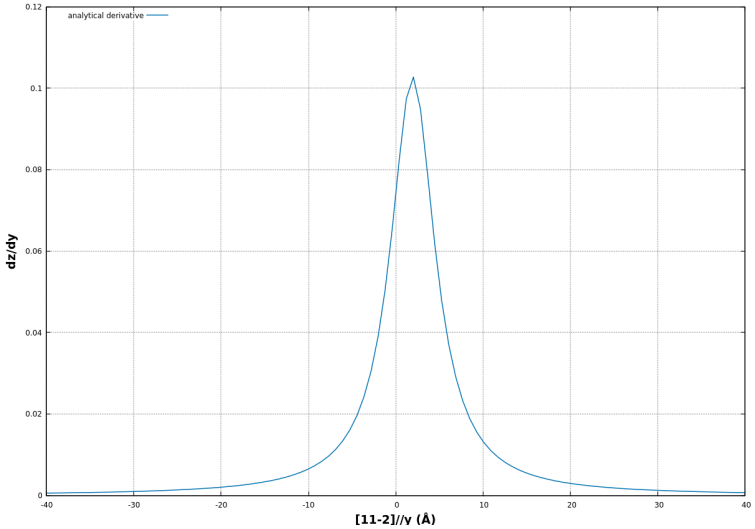

Figure 5.33: Analytical derivative of z=f(y) indicates the position of one of the three $\frac{\alpha}{6}[111]$ partial dislocation in tungsten.

is in agreement with elastic prediction:

$$b_p^2 = \frac{a^2}{36}(1^2 + 1^2 + 1^2) = 0.912\mathring{A}$$

Therefore, the effective position of one of the three dislocation is $x_0 = 1.936$ Å in y-direction. The dislocation dissociates to {112} planes.

The elastic strain energy in crystal tungsten containing the three partial dislocations in shown in Figure 5.34. The fitting to the data yields almost identical results as in the case of the perfect $\frac{a}{2}[111]$ dislocation. The slope of the line is a=22.5951 and y-intercept is b=1.71302. Therefore, the shear modulus of the tungsten with three partial screw dislocations is :

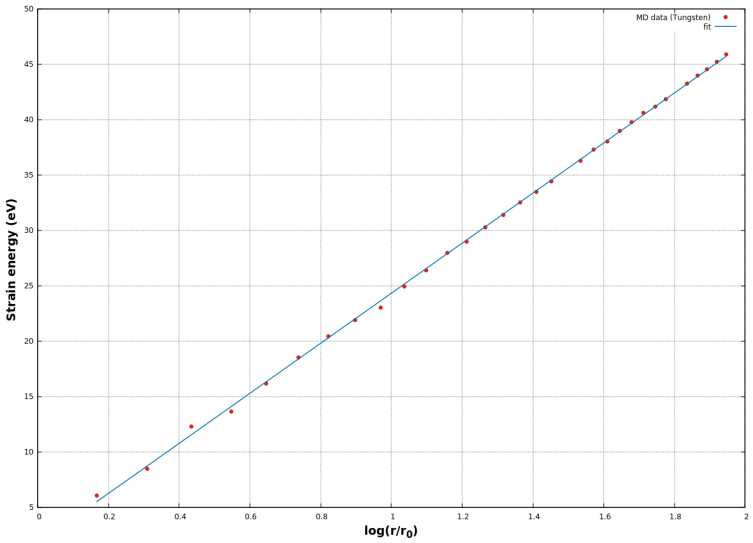

Figure 5.34: Elastic strain energy in cylindrical shells of outer radius r and inner radius r_0 containing three $\frac{\alpha}{6}[111]$ partial dislocations in tungsten (W).

$$\frac{Gb^2}{4\pi} = \frac{a}{L} \Rightarrow \frac{4 \times \pi \times 22.5951eV}{(2.735)^2} \times 38.29\mathring{A}^3 \Rightarrow G = 0.9913ev/\mathring{A}^2$$

or

$$G = C_{44} = 158.61GPa$$

Finally, the dislocation in W was equilibrated to 300K in the (NVT) ensemble. The dissociated screw dislocation stays stable in the simulation cell at finite temperature in bcc metals as well as in fcc metals as shown in Figure 5.35.

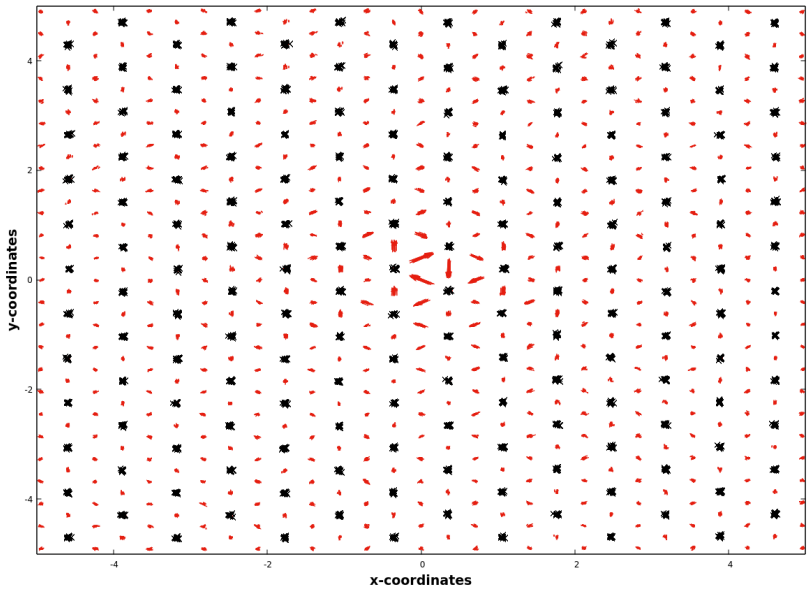

Figure 5.35: DDM of the dissociated screw dislocation in W at 300K

Table 5.1: Shear modulus and C_{44} calculated in current work compared to the experimental values

el/ment	G (GPa)	G_{exper} (GPa) [37]	C_{44} (GPa)	C_{44} GPa
Cu	55.83	45	97.85	75.4 [38]
Al	28.54	27	29.46	28.3 [39]
W	158.61	161	159.6	163.8 [40]

5.3 Discussion

We introduced perfect screw dislocations in three metals: aluminum, copper and tungsten. The models take the elastic anisotropy into account. Thus, aluminum and tungsten are isotropic and copper shows highly anisotropic behavior. We calculated the distance dependence of elastic strain energy in respect to the dislocation centre. From this relation we obtained the shear modulus as the elastic strain energy has a linear dependence to the logarithm of r. For isotropic materials shear modulus coincides with the elastic constant C_{44} while for anisotropic materials shear modulus has to be multiplied by the anisotropy factor to give the elastic constant C_{44}. The calculated values of shear modulus and C_{44} for Al (26880 atoms), Cu and W are shown in Table (6.1).

After relaxation, for all three cases, perfect screw dislocation dissociates into partial dislocations. In fcc Al and Cu perfect screw dislocation dissociates into co-planar Shockley partials as expected. The dissociation width between them was found and the SFEs were calculated $129mJ/m^2$ for Al and $48mJ/m^2$ for Cu in agreement with model's parameters ($141mJ/m^2$ for and $45mJ/m^2$ for Cu). In bcc W perfect screw dislocation dissociates into three non co-planar partial screw dislocations. Therefore the same methology of calculating the SFE was not applicable. The partial dislocations were identified. The calculated SFEs are in good comparison with DFT simulation results where the stacking fault energy of Al is $162mJ/m^2$ [41] and of Cu $41mJ/m^2$. [42]

To identify the finite size effects the dissociation width r_{eq} in Al was calculated additionally for systems of 9216 atoms with $L_x \approx L_y \approx 79$ Å and 38016 atoms with $L_x \approx L_y \approx 162$ Å. The dissociation widths were found 5.17 Å and 7.62 Å respectively. A graph of the dissociation width with respect to 1/L is shown in Figure 5.36. The y-intercept of linear function would give the dissociation width in the case of "infinitely" large system. For the graph of Figure 5.36 the y-intercept is found 9.87 Å in good agreement with the elastic prediction of 10.47Å calculated from Equation (3.11).

The above method of calculating the elastic constant C_{44} was compared to the central difference method for the isotropic case of Al as for isotropic media $C' \approx C_{44}$. Different values of strain were applied on a Al crystal of 16128 atoms in a simulation cell of $80 \times 80 \times 40$ Å at 0K. The energy density is given from the

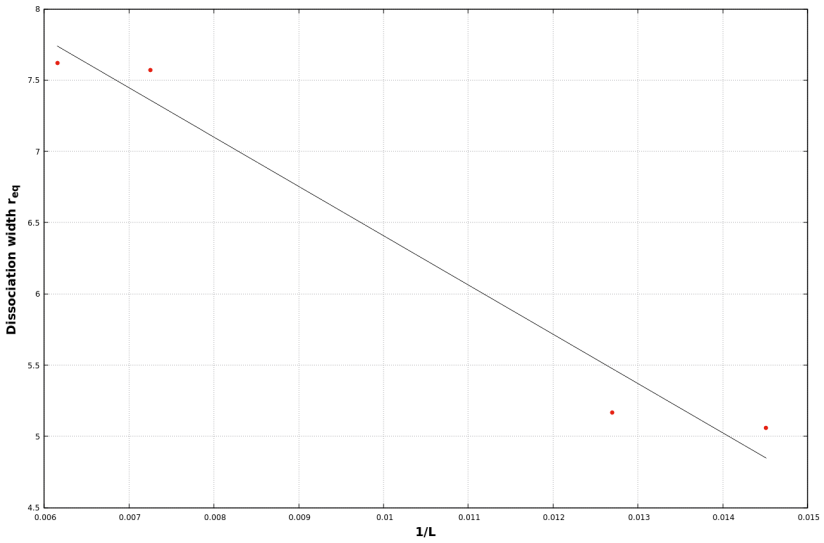

Figure 5.36: Dissociation width in Al as a function of inverse box length L in x-, y-direction

Equation (2.13). So, if we suppose only pure shear $\epsilon_{zz} = 0$, it is then

$$U_{el} = \frac{1}{2}(2\epsilon^2)C_{11} + C_{12}(-\epsilon^2) = (C_{11} - C_{12})\epsilon^2$$

$$\frac{\partial U_{el}}{\partial \epsilon} = 2\epsilon C_{11} - 2C_{12}\epsilon \Rightarrow \frac{\partial^2 U_{el}}{\partial \epsilon^2} = 2(C_{11} - C_{12})$$

$$C_{11} - C_{12} = \frac{1}{2}\frac{\partial^2 U_{el}}{\partial \epsilon^2}$$

But $C' = \frac{1}{2}(C_{11} - C_{12})$, so

$$C' = \frac{1}{4}\frac{\partial^2 U_{el}}{\partial \epsilon^2}$$

The calculation of the second derivative of the elastic energy U with respect to the strain is given the following way. We consider the Taylor expansion series of U about ϵ and -ϵ.

$$U(\epsilon) = U(0) + \epsilon U'(0) + \epsilon + \epsilon^2 U''(0)/2! + \epsilon^3 U'''(0)/3! + O(\epsilon^4)$$

$$U(\epsilon) = U(0) - \epsilon U'(0) + \epsilon + \epsilon^2 U''(0)/2! + \epsilon^3 U'''(0)/3! + O(\epsilon^4)$$

By considering terms only to the second order, we add the above two equations. The second derivative is given by

$$\frac{\partial^2 U_{el}}{\partial \epsilon^2} = \frac{U(\epsilon) + U(-\epsilon) - 2U(0)}{\epsilon^2} + O(\epsilon^4)$$

In Figure 5.37 the calculated values of C' are shown for several strain values between between 5×10^{-4} and 1×10^{-1}. We see that the value of C' converges to $[30.3 - 30.9]$ GPa for ϵ between 10^{-3} and 2×10^{-2}. This result is in good agreement with the calculated value of $C_{44} = 29.46$ GPa in Al (26880 atoms) from the screw

dislocation energy at 0K.

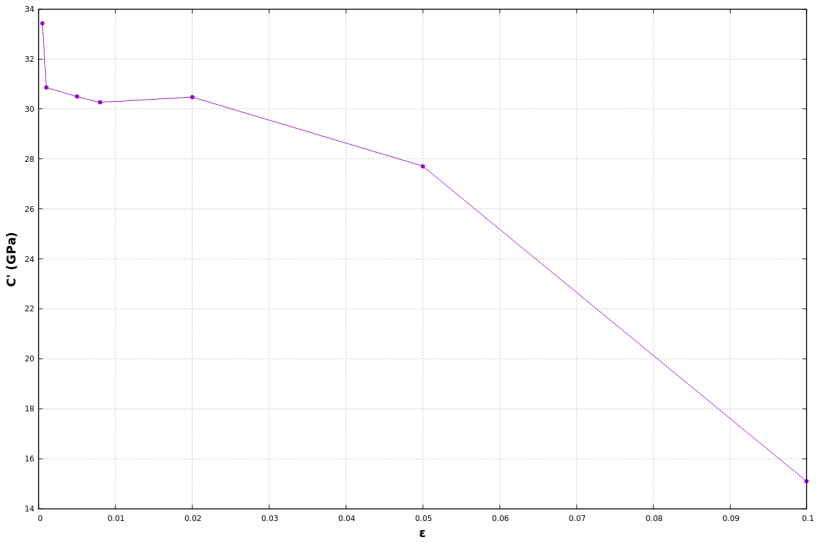

Figure 5.37: C' calculated from pure shear applied in Al at 0K

Chapter 6

Concluding remarks

Overall the use of Helicoidal Boundary Conditions in the simulation of dislocations is successful. From the introduction of screw dislocation in fcc and bcc metals and its properties we calculated the shear modulus and elastic constant C_{44} in good agreement with the bibliography and experimental results. The results are specially good for the isotropic cases of Al (fcc) and W (bcc) but diverge for the case of Cu (fcc). That probably is due to the interatomic potential. This method of calculating the C_{44} is advantageous in comparison to the central difference method as disscused above as it is faster, no need to apply different strains and find the plateu, and can be performed at finite temperatures.

In fcc metals, where the perfect screw dislocations dissociate into co-planar Shockley partials, we found the effective positions of the partial screw dislocations and calculated the stacking fault energies (SFEs) of Al and Cu in good agreement with other simulation works. In the bcc metal, the perfect screw dislocation dissociates into three partial dislocations successfuly as predicted using a new interatomic potential for W that has been proved to give very realistic results for this kind of work. That could set the base for a future work to explain the brittle-to-ductile transition of Tungsten at extreme cold temperatures.

The biggest advantages of the Helical Boundary Conditions in the dislocation simulation are the fast equilibration time ($\sim 10^3$ timesteps) and the use of small simulation cells. Of course, by increasing the simulation cell in x,y-directions one can get closer values, i.e.the dissociation width, to the elastic prediction. Additionally, the maintenance of the dislocations in the simulation cell at finite temperature is another important outcome of the application of HBC.

Appendix A

Tungsten Potential

This model potential for tungsten was implemented implemented using the Linear Combination Atomic Orbital (LCAO) method and adjusting to experimental values.

$$U_i = A_{SR}\sum_{j\neq i}(1-\frac{r_{ij}}{\rho_{SR}})+A_{6s}^{TF}(\sum_{j\neq i}f_d^s(r_{ij})\rho_{6s}(r_{ij}))^{5/3}+\xi_{5d}(\sum_{j\neq i}f_d^d(r_{ij})\rho_{5d}(r_{ij}))^{1/2}+\xi_{6s}(\sum_{j\neq i}f_d^d(r_{ij})\rho_{6s}(r_{ij}))^{1/2}$$

Fist term is the repulsion hard-core, approximately zero if $r_{ij} > \rho_{SR}$. The second term is the Thomas-Fermi repulsion. The third and fourth terms correspond to the tight-binding attraction of electron d and for tight0-binding attraction of electron s respectively.

The screening function Fermi-Dirac is

$f_d(r_{ij}) = \frac{1}{1+\exp(\epsilon(\frac{r_{ij}}{r_c}-1))}$

for which ϵ and r_c are different for 6s or 5d electrons, and

$\rho_{5d}(r_{ij}) = [(B_0 - B_1\rho^* + \rho^{*2}) \times a_N \times {Z^*}_d^{3/2} \times \rho^{*2}\exp(-\rho^2 * /2)]^2$

$B_0 = 42,\ B_1 = 14$

$a_N = \frac{1}{150\sqrt{70}}$

$\rho* = \frac{zZ_d^*}{5}\frac{r_{ij}}{\alpha_{Bohr}}$, $a_{Bohr} = 0.529177$ Å

$\rho_{6s}(r_{ij}) = [(B_0 - B_1\rho^* + \rho^{*2} + B_2\rho^{*2} - B_3\rho^{*3} + B_4\rho^{*4} - r^{*5}) \times a_N \times Z_s^*]^2$

$B_0 = 720, B_1 = 1800, B_2 = 1200, B_3 = 300, B_4 = 30, \alpha_N = \frac{1}{2160\sqrt{6}}$

$\rho^* = \frac{zZ_s^*}{6}\frac{r_{ij}}{\alpha_{Bohr}}$

Bibliography

[1] M. Parrinello and A. Rahman. Strain fluctuations and elastic constants. *The Journal of Chemical Physics*, 76(5):2662–2666, 1982.

[2] John R. Ray and A. Rahman. Statistical ensembles and molecular dynamics studies of anisotropic solids. *The Journal of Chemical Physics*, 80(9):4423–4428, 1984.

[3] John R. Ray, Michael C. Moody, and Aneesur Rahman. Molecular dynamics calculation of elastic constants for a crystalline system in equilibrium. *Phys. Rev. B*, 32:733–735, Jul 1985.

[4] Kevin Van Workum and Juan J. de Pablo. Improved simulation method for the calculation of the elastic constants of crystalline and amorphous systems using strain fluctuations. *Phys. Rev. E*, 67:011505, Jan 2003.

[5] Surajit Sengupta, Peter Nielaba, Madan Rao, and K. Binder. Elastic constants from microscopic strain fluctuations. *Phys. Rev. E*, 61:1072–1080, Feb 2000.

[6] E. Orowan. Zur kristallplastizität. iii. *Zeitschrift für Physik*, 89:634–659, 1934.

[7] M. Polanyi. Über eine art gitterstörung, die einen kristall plastisch machen könnte. *Zeitschrift für Physik*, 89:660–664, 1934.

[8] Geoffrey Ingram Taylor. The mechanism of plastic deformation of crystals. part i. theoretical. *Proceedings of the Royal Society of London. Series A, Containing Papers of a Mathematical and Physical Character*, 145(855):362–387, 1934.

[9] J. P. Hirth and J. Lothe. *Theory of Dislocations*. New York: Wiley, 1982.

[10] L. D. Landau and E. M. Lifshitz. Theory of elasticity. In *Course of Theoretical Physics*, pages 1–15. Pergamon Press, 1975.

[11] E.M. Lifshitz, A.M. Kosevich, and L.P. Pitaevskii. Chapter i - fundamental equations. In E.M. Lifshitz, A.M. Kosevich, and L.P. Pitaevskii, editors, *Theory of Elasticity)*, pages 1 – 37. Butterworth-Heinemann, Oxford, third edition, 1986.

[12] D. Hull and D. J. Bacon. *Introduction to Dislocations*. Elsevier Ltd., fifth edition edition, 2011.

[13] D. Rodney and J. Bonneville. Dislocations. In David E. Laughlin and Kazuhiro Hono, editors, *Physical Metallurgy*, volume 2, pages 1591–1674. Elsevier, fifth edition edition, 2014.

[14] C R Weinberger, B L Boyce, and C C Battaile. Slip planes in bcc transition metals. *International Materials Reviews*, 58(5):296–314, 2013.

[15] W. Cai, J. Li V V Bulatov, J. Chang, and S. Yip. Dislocation core effects on mobility. In F.R.N. Nabarro and J.P. Hirth, editors, *Dislocations in Solids*, volume 12, chapter 64, pages 1–80. Elsevier, Amsterdam, 2004, 2004.

[16] V. Vitek and F. Kroupa. Generalized splitting of dislocations. *The Philosophical Magazine: A Journal of Theoretical Experimental and Applied Physics*, 19(158):265–284, 1969.

[17] M. S. Duesbery and G. Y. Richardson. The dislocation core in crystalline materials. *Critical Reviews in Solid State and Materials Sciences*, 17(1):1–46, 1991.

[18] M.S. Duesbery and V. Vitek. Plastic anisotropy in b.c.c. transition metals. *Acta Materialia*, 46(5):1481 – 1492, 1998.

[19] Wei Cai and William D. Nix. *Imperfections in Crystalline Solids*. Cambridge University Press, 2016.

[20] B. J. Alder and T. E. Wainwright. Phase transition for a hard sphere system. *The Journal of Chemical Physics*, 27(5):1208–1209, 1957.

[21] B. J. Alder and T. E. Wainwright. Studies in molecular dynamics. i. general method. *The Journal of Chemical Physics*, 31(2):459–466, 1959.

[22] John A. Moriarty, Vaclav Vitek, Vasily V. Bulatov, and Sidney Yip. Atomistic simulations of dislocations and defects. *Journal of Computer-Aided Materials Design*, 9:99–132, 2002.

[23] Loup Verlet. Computer "experiments" on classical fluids. i. thermodynamical properties of lennard-jones molecules. *Phys. Rev.*, 159:98–103, Jul 1967.

[24] Fabrizio Cleri and Vittorio Rosato. Tight-binding potentials for transition metals and alloys. *Phys. Rev. B*, 48:22–33, Jul 1993.

[25] Vasily Bulatov and Wei Cai. *Computer Simulations of Dislocations (Oxford Series on Materials Modelling)*. Oxford University Press, Inc., USA, 2006.

[26] A. Aslanides and V. Pontikis. Atomistic study of dislocation cores in aluminium and copper. *Computational Materials Science*, 10(1):401 – 405, 1998. Computational Modelling of Issues in Materials Science.

[27] Vassilis Pontikis, Gianguido Baldinozzi, Laurence Luneville, and David Simeone. Near transferable phenomenologicaln-body potentials for noble metals. *Journal of Physics: Condensed Matter*, 29(35):355701, jul 2017.

[28] Model box periodic boundary conditions -p.b.c. http://isaacs.sourceforge.net/phys/pbc.html. Accessed: 2021-02-06.

[29] M. E. J. Newman and G. T. Barkema. *Monte Carlo Methods in Statistical Physics*. Oxford University Press, Inc., USA, 1999.

[30] Anjan Chandra and Subinay Dasgupta. Multidimensional persistence behavior in an ising system. *Physical review. E, Statistical, nonlinear, and soft matter physics*, 77:031111, 04 2008.

[31] Shichi Nose. A molecular dynamics method for simulations in the canonical ensemble. *Molecular Physics*, 52(2):255–268, 1984.

[32] William G. Hoover. Canonical dynamics: Equilibrium phase-space distributions. *Phys. Rev. A*, 31:1695–1697, Mar 1985.

[33] Hans C. Andersen. Molecular dynamics simulations at constant pressure and/or temperature. *The Journal of Chemical Physics*, 72(4):2384–2393, 1980.

[34] V. Vitek, R. C. Perrin, and D. K. Bowen. The core structure of (111) screw dislocations in b.c.c. crystals. *The Philosophical Magazine: A Journal of Theoretical Experimental and Applied Physics*, 21(173):1049–1073, 1970.

[35] J. W. Steeds. *Introduction to Anisotropic Elasticity Theory of Dislocations*. Clarendon Press - Oxford, 1973.

[36] D. Mordehai, Y. Ashkenazy, I. Kelson, and G. Makov. Dynamic properties of screw dislocations in cu: A molecular dynamics study. *Phys. Rev. B*, 67:024112, Jan 2003.

[37] Engineering Toolbox. Modulus of rigidity. https://www.engineeringtoolbox.com/modulus-rigidity-d_946.html, 2005. Accessed: 2021-02-06.

[38] H. M. Ledbetter and E. R. Naimon. Elastic properties of metals and alloys. ii. copper. *Journal of Physical and Chemical Reference Data*, 3(4):897–935, 1974.

[39] J. Vallin, M. Mongy, K. Salama, and O. Beckman. Elastic constants of aluminum. *Journal of Applied Physics*, 35(6):1825–1826, 1964.

[40] F.H. Featherston and J.R. Neighbours. Elastic constants of tantalum, tungsten, and molybdenum, 1963.

[41] Marek Muzyk, Zbigniew Pakiea, and Krzysztof J. Kurzydowski. Generalized stacking fault energies of aluminum alloysdensity functional theory calculations. *Metals*, 8(10), 2018.

[42] P. S. Branicio, J. Y. Zhang, and D. J. Srolovitz. Effect of strain on the stacking fault energy of copper: A first-principles study. *Phys. Rev. B*, 88:064104, Aug 2013.

List of Figures

2.1 Shear displacements u_1 and u_2 and angles of shear ϕ_1 and ϕ_2 [9] 8

2.2 Stress distribution on a infitensimal volume element [9] 9

3.1 (a) Model of simple cubic lattice (b) Edge dislocation DC formed by inserting an extra half-plane of atoms in ABCD [12] 14

3.2 (a) A left-hand screw dislocation (b) A right-hand screw dislocation [12] 14

3.3 Burgers circuit about an edge dislocation [9] 15

3.4 (a) Screw dislocation AB formed in a crystal (b) Elastic distortion of a cylindrical tube simulating the distortion produced by the screw dislocation [12] 17

3.5 Slip of {111} planes in face-centeed cubic metals [12] 19

3.6 Dissociation of a perfect dislocation into Shockley partials [9] 19

3.7 Stacking of BCC structure (a) Three-dimensional view (b) Plan view [19] 21

3.8 The $(1\bar{1}2)$ planes of a bcc crystal showing the six layers comprising the ABCDEF... stacking sequence. [19] 22

3.9 BCC crystal viewed along the [110] direction, showing the stacking sequence on the $(1\bar{1}2)$ plane (a) Perfect stacking sequence ABCDEF... (b) If the layer slips relative to layer A by $\frac{\alpha}{6}[\bar{1}11]$, it becomes layer Fcreating an intristic stacking fault [19] 22

4.1 Periodic Boundary Conditions. Images of the simulation box (in the centre) are attached side by side in all dimensions. When a particle leaves the box from one side, it re-enters from the opposite one with the same velocity. [28] 28

4.2 Two dimensional lattice with helicoidal boundary conditions. [30] 29

5.1 DDM of the screw dislocation before damping (Al 6720 atoms) 32

5.2 Energy per atom in x-y plane around a perfect screw dislocation at 0K (Al 6720 atoms) . . . 32

5.3 z coordinate as function of y on {111} plane after the screw dislocation was introduced (Al 6720 atoms) 33

5.4 Analytical derivative of z=f(y) indicates the position of an $\frac{1}{2}[1\bar{1}0]$ screw dislocation (Al 6720 atoms) . . . 34
5.5 The strain energy within a cylinder of radius R that contains a screw dislocation along its axis (Al 6720 atoms) . . . 34
5.6 DDM of the dissociated screw dislocation after damping at 0K (Al 6720 atoms) . . . 35
5.7 Site energies in x-y plane around a dissociated screw dislocation at 0K (Al 6720 atoms) . . . 35
5.8 z coordinate as function of y on {111} plane in the relaxed configuration of 6720 atoms . . . 36
5.9 Analytical derivative of z=f(y) indicates the positions of the Shockley partials (6720 atoms) . 36
5.10 The strain energy within cylindrical shells containing two partial dislocations(6720 atoms) . . 37
5.11 DDM of a perfect screw dislocation at 400K (Al 6720 atoms) . . . 38
5.12 DDM of the dissociated screw dislocation at 400K (Al 6720 atoms) . . . 38
5.13 The strain energy within cylindrical shells of outter r and inner radius r_0 with a $\frac{1}{2}[1\bar{1}0]$ screw dislocation (Al 26880 atoms) . . . 38
5.14 z=f(y) on a {111} plane in relaxed configuration (Al 26880 atoms) . . . 40
5.15 Analytical derivative of z=f(y) indicates the effective positions of the Shockley partiasl (Al 26880 atoms) . . . 40
5.16 The strain energy in cylindrical shells around Shockley partials(Al 26880 atoms) . . . 41
5.17 DDM around a $\frac{\alpha}{2}[110]$ screw dislocation in Cu viewed from [110] direction . . . 41
5.18 Energy per atom in x-y plane around a perfect screw dislocation at 0K in copper . . . 41
5.19 The elastic strain energy in copper containing a $\frac{1}{2}[111]screwdislocation$ . . . 42
5.20 DDM of Shockely partials in Cu . . . 42
5.21 Energy per atom in Cu containing Shockley partials . . . 42
5.22 z=f(y) viewed from [111] direction in Cu with Shockley partials . . . 43
5.23 Numerical derivative of z=f(y) indicates the effective positions of the Shockley partials in Cu 43
5.24 The strain energy within cylindrical shells containing Shockley partials in anisotropic copper. 44
5.25 DDM of a perfect screw dislocation in copper at 400K . . . 44
5.26 DDM of a disscociated screw dislocation in copper at 400K . . . 44
5.27 DDM of a perfect screw dislocation in Tungest (bcc) of Burgers vector $\frac{\alpha}{2}[111]$ . . . 45
5.28 z coordinate as function of x on {111} plane before relaxation . . . 46
5.29 Analytical derivative of z=f(x) indicates the position of the screw dislocation in tungsten (W) 46
5.30 The strain energy within a cylindrical shell of inner radius r and outer radius r_0 along a screw dislocation $\frac{\alpha}{2}[111]$ in W . . . 47
5.31 Displacement map of three partial $\frac{\alpha}{6}[111]$ screw dislocations in W . . . 47
5.32 z=f(y) in tungsten (W) viewed from [110] direction. . . . 48

5.33 Analytical derivative of z=f(y) indicates the position of one of the three $\frac{\alpha}{6}[111]$ partial dislocation in tungsten. 48

5.34 Elastic strain energy in cylindrical shells of outer radius r and inner radius r_0 containing three $\frac{\alpha}{6}[111]$ partial dislocations in tungsten (W). 49

5.35 DDM of the dissociated screw dislocation in W at 300K 49

5.36 Dissociation width in Al as a function of inverse box length L in x-, y-direction 51

5.37 C' calculated from pure shear applied in Al at 0K 52

List of Tables

4.1 Parameters of TBSMA potential model for Al and Cu. 27

5.1 Shear modulus and C_{44} calculated in current work compared to the experimental values . . . 50